DEVELOPMENT OF AN IMPROVED ALGORITHM FOR MULTIPLE DIFFRACTIONS IN URBAN RADIO PROPAGATION

A THESIS SUBMITTED TO

THE GRADUATE SCHOOL OF NATURAL AND APPLIED SCIENCES

OF

ATILIM UNIVERSITY

BY

MEHMET BARIŞ TABAKCIOĞLU

IN PARTIAL FULFILLMENT OF THE REQUIREMENTS FOR THE DEGREE OF

MASTER OF SCIENCE

IN

THE DEPARTMENT OF ELECTRICAL AND ELECTRONICS ENGINEERING

JANUARY 2009

Approval of the Graduate School of Natural and Applied Science, Atılım University

Prof. Dr. Abdurrahim Özgenoğlu

Director

I certify that this thesis satisfies all the requirements as a thesis for the degree of Master of Science.

Asst. Prof. Dr. Ali Kara

Head of Department

This is to certify that we have read this thesis and that in our opinion it is fully adequate, in scope and quality, as a thesis for the degree of Master of Science.

Asst. Prof. Dr. Ali Kara

Supervisor

Examining Committee Members

Assoc. Prof. Dr. Çiğdem Seçkin Gürel _____

Asst. Prof. Dr. Bülent Tavlı _____

Asst. Prof. Dr. Nursel Akçam _____

Asst. Prof. Dr. Elif Uray Aydın _____

Asst. Prof. Dr. Ali Kara _____

Date: 19.01.2009

I declare and guarantee that all data, knowledge and information in this document has been obtained, processed and presented in accordance with academic rules and ethical conduct. Based on these rules and conduct, I have fully cited and referenced all material and results that are not original to this work.

Mehmet Barış Tabakcıoğlu

ABSTRACT

DEVELOPMENT OF AN IMPROVED ALGORITHM FOR MULTIPLE DIFFRACTIONS IN URBAN RADIO PROPAGATION

Tabakcıoğlu, Mehmet Barış

M.S., Electrical and Electronics Engineering Department

Supervisor: Asst. Prof. Dr. Ali Kara

January 2009, 70 pages

This thesis presents a review of diffraction algorithms based on Uniform Theory of Diffraction (UTD) for multiple diffractions, and proposes an improved UTD model for fast and more accurate field prediction for multiple diffractions. The proposed model is based on the improved version of slope UTD and Fresnel zone concept, called slope UTD with convex hull. This model can be used for coverage prediction in terrestrial broadcasting systems. The thesis also provides a comparison for UTD based algorithms, and discusses the results for computation time and accuracy. Furthermore, slope UTD and slope UTD with convex hull models are compared with a Physical Optics (PO) solution based on numerical computation of Kirchhoff-Huygens integrals. Results of extensive simulations are presented, and discussed for the development of fast and accurate radio network planning tools.

Keywords: slope UTD, multiple diffraction, Fresnel zones, Geometrical theory of diffraction

ÖZ

KENTSEL RADYO YAYILIMINDA ÇOKLU KIRINIMLAR İÇİN İYİLEŞTİRİLMİŞ BİR ALGORİTMA GELİŞTİRİLMESİ

Tabakcıoğlu, Mehmet Barış

Yüksek Lisans, Elektrik-Elektronik Mühendisliği Bölümü

Tez yöneticisi: Yard. Doç. Dr. Ali Kara

Ocak 2009, 70 sayfa

Bu tezde, çoklu bina yapılarında geçiş bölgesi kırınımları için Genel Kırınım Teorisine (GKT) dayalı kırınım algoritmaları özetlendi ve çoklu bina yapılarında elektrik alan tahmini için daha hızlı ve kesin sonuçlar veren daha gelişmiş bir GKT algoritması ileri sürüldü. Dışbükey zarf tekniğine dayalı eğim kırınımı modeli (EKDZ), Eğim kırınımı (EK) ve fresnel bölgesi kavramı üzerine kurulmuştur. Bu model karasal yayıncılıkta kapsama alanı kestiriminde de kullanılabilir. Bu tez ayrıca, GKT bazlı modelleri hesaplama süresi ve kesinlik için karşılaştırır. Üstelik, EK ve EKDZ modelleri, Kirchhoff-Huygens integrallerinin çözümü üzerine kurulan fiziksel optik modeli ile de karşılaştırılır. Daha hızlı ve kesin radio ağları planlaması yapmak için çok geniş çaptaki benzetimlerin sonuçları sunuldu ve tartışıldı.

Anahtar Kelimeler: Eğim Kırınımı, çoklu kırınım, fresnel bölgeleri, Geometrik kırınım teorisi.

To My Parents and brothers

ACKNOWLEDGEMENTS

I express sincere appreciation to my supervisor Assist. Prof. Dr. Ali Kara for his guidance and insight throughout the research. Thanks also go to Ahmet Özmen and Mustafa Aslanbek Kılıçarslan for their assist on programming. To my all brothers, especially Serkan Yeşilova, Nedim Arın and Ahmet Emre Tekeli, I offer sincere thanks for their continuous support and patience during this period. Special thanks go to Ali Yüklü, Ahmet Köseoğlu, Murat Devecioğlu, Ali Engin, Ahmet Enes Demir and Kadir Polat for their friendship and help during my work.

This study has been carried out at Electrical-Electronics Engineering Department of Atılım University as “Development of Radio Propagation Model based on Slope Diffraction and Convex Hull Techniques” Project during the years 2006-2008. This Project, 105E083, has been supported by TÜBİTAK (The Scientific and Technological Research Council of Turkey).

TABLE OF CONTENTS

LIST OF TABLES

TABLES

LIST OF FIGURES

FIGURES

LIST OF SYMBOLS

L - Distance parameter for amplitude diffraction coefficient

L_s - Distance parameter for slope diffraction coefficient

A(s) – Spreading factor

D_s – Amplitude diffraction coefficient for soft polarization

D_h - Amplitude diffraction coefficient for hard polarization

F(x) – Transition function

β – interior angle

R_{0h} –Reflection coefficient for hard polarization, from 0-face

R_{0s} - Reflection coefficient for soft polarization, from 0-face

R_{nh} - Reflection coefficient for hard polarization, from n-face

R_{ns} - Reflection coefficient for soft polarization, from n-face

ε_r – Relative permittivity constant

d_s – Slope diffraction coefficient

μ - mean

σ - standard deviation

LIST OF ABBREVIATIONS

UHF- Ultra High Frequency

UTD- Uniform Theory of Diffraction

S-UTD- Slope UTD

S-UTD-CH- Slope UTD with Convex Hull

PO- Physical Optic

3D- Three Dimension

MHz- Mega Hertz

km- kilometer

dB- deci bell

LOS- Line of Sight

2D- Two Dimension

GHz- Giga Hertz

TRW- Transition Region Width

IDE- Isolated diffracting Edge

GO- Geometrical Optic

BS- Base Station

MS- Mobile Station

GTD- Geometrical Theory of diffraction

RPL- Relative Path Loss

PL- Path Loss

FL- Free Space Loss

CHAPTER 1

INTRODUCTION

To make more reliable and efficient digital communication networks and broadcasting systems, accurate and time efficient theoretical models being capable of generating field predictions, are proposed. Many propagation prediction models have been proposed for prediction of field strengths for different environments as classified as indoor, urban, suburban or rural areas. In general, these models can be classified as numerical models and ray theoretical models. While numerical models look for numerical solutions to some integrals, ray theoretic models rely on ray tracing algorithms.

Ray tracing has been promising technique and has widely been used for channel studies in indoor and outdoor wireless communication systems. In rural areas, propagation prediction models have traditionally treated obstacles in the terrain as knife edges or wedges for UHF and microwave ranges [1]. Mountain and hill can be modeled as wedge type of obstacle, whereas building as knife-edge type of obstacle. Then, multiple-diffraction problems have been investigated for a long time, and Uniform Theory of Diffraction (UTD) based models have been proposed to predict the field strength in the urban and suburban environments.

Although classical UTD model [2] is time efficient for multiple-diffraction it fails to predict the field strength accurately even if one obstacle is placed in the transition zone of the neighboring obstacle. Detailed information and simulation results for UTD are presented in chapter 2. UTD is acceptable model due to its lower computation time in only the case that difference between obstacle heights is very high. UTD can also be used coverage prediction in broadcasting systems. In other words, as obstacle heights are approximately equal, UTD fails to predict the field strength accurately.

An improved UTD based multiple diffraction model [3, 4] is proposed to predict the field strength accurately with lower computation time. The deficiency of this model is that the model works for only in the case that obstacles have equal heights and spacing and is also based on only amplitude diffraction effects.

A more accurate model [5] for field prediction based on classical UTD model has been proposed by including slope diffraction terms, so-called slope UTD, (S-UTD). The insufficiency of the model [5] is that the phase continuity is not met resulting discontinuities in the transition zone in calculation of the distance parameters L and L_s for amplitude and slope diffraction coefficient. In chapter 3, there are simulations showing the difference between the models [2] and [5].

To solve this problem another improvement on UTD based model is proposed [6] with adding the higher order diffracted fields for multiple-diffraction. Even though this model is ultimately accurate; its computation complexity is very high. Yet, can still be used as a reference.

An improved version of S-UTD model is proposed [7, 8] where it has claimed that the phase continuity should be met in calculating the distance parameters L and L_s appearing in the amplitude and the slope diffraction coefficients. Improved version of S-UTD model has given acceptable results in comparison with Vogler's model [9] which is known to be ultimately accurate. Detailed information about the improved model and simulation results for comparison with model in [5] is given in chapter 3. Moreover, calculation of the distance parameters for the amplitude and slope diffraction coefficient is given in appendix B. Although, S-UTD model has shown to deal with multiple diffraction problems, its validity has been reported to be limited in the number of diffractions [10].

On the other hand, some numerical models have already been proposed for field prediction in multiple diffraction problems. Among these models, one based on direct numerical solution of Kirchhoff-Huygens integrals is presented in [11].

Another numerical model proposed in [9] was based on numerical solution of multiple Fresnel like integrals. It has usually been discarded for practical system prediction, due to the computation time required and the complexity of implementation [12].

Numerical models treat more realistic scenarios and produce very accurate results but are very time-inefficient when the number of obstacles increases. UTD based models are known with very time efficient in urban propagation modeling. Then, there are trade-offs between computation time and accuracy of field prediction and between computation complexity and the accuracy of field prediction of models. Models having higher accuracy with large computation time seem to be infeasible in many cases.

Another UTD based ray theoretical model is proposed to predict the field strength accurately in this thesis. The proposed model is an improvement for the model [7, 8], is called slope UTD with Convex Hull model (S-UTD-CH) [13-18]. S-UTD-CH model combines S-UTD model and Fresnel zone concept in order to eliminate some of the diffracting obstacles before S-UTD model implementation, and reduce the computation time of S-UTD model by reducing the number of diffractions. Moreover, a ray tracing algorithm is developed to determine all rays contributing to the total field for multiple diffraction geometries. Besides an algorithm is developed for calculating the transition function is given in appendix A. Furthermore, this model can be used for prediction of coverage in terrestrial broadcasting systems. Extensive simulation results in chapter 4 showed that S-UTD-CH model is a highly optimal model due to its computation time and accuracy of field prediction. Simulation results for statistical comparison of UTD based models; (UTD, S-UTD and S-UTD-CH) are given in chapter 5. Finally, statistical comparison of S-UTD/S-UTD-CH models with a numerical model named Physical Optics (PO) model based on Kirchhoff-Huygens approximation [11] (chapter 5) is presented for the first time in this thesis.

Furthermore, 3D ray tracing techniques and models for field prediction are given (chapter 6) as area of future work. Finally, brief information about models, comparison results of models and usage area of models are given (chapter 7).

CHAPTER 2

UNIFORM THEORY OF DIFFRACTION (UTD)

Uniform Theory of diffraction (UTD) model has been used for a long time for field prediction and coverage prediction in terrestrial broadcasting systems. This model can be used with higher accuracy and lower computation time, if the difference between obstacles is large.

In this chapter, classical UTD formulation is reviewed, transition regions problem is defined, and some test cases and validations are presented. Most of the test cases are taken from the literature as described.

According to the UTD [2] formulation, the diffracted field behind an obstacle is given by

$$E = [E_i D]A(s)e^{-jks} \tag{1}$$

where, E_i is the incident field. D is amplitude diffraction coefficient. $A(s)$ is the spreading factor, k is wave number and s is difference between obstacle and the receiver.

Spreading factor is given [1] by

$$A(s) = \sqrt{\frac{s_0}{s(s_0+s)}} \tag{2}$$

where, s_0 is total distance between the transmitter and the obstacle as shown in Fig. 1.

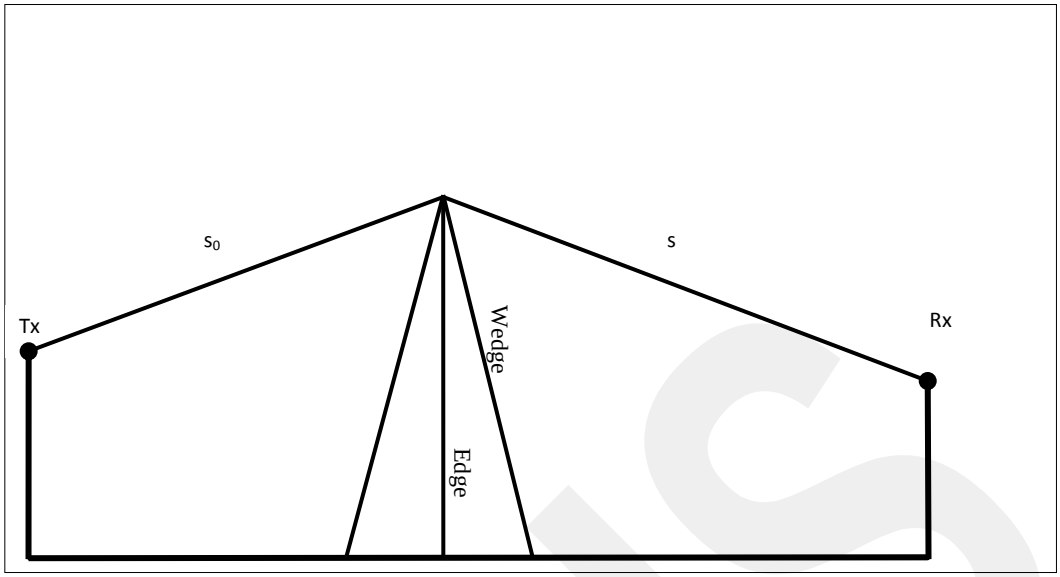

Fig.1. Knife-edge or wedge type of obstacle

D appearing in the equation (1), which is the amplitude diffraction coefficient for wedge type of obstacle, is given [19] by

$$D_s = R_{0s}R_{ns}D_1 + D_2 + R_{0s}D_3 + R_{ns}D_4 \tag{3-a}$$

$$D_h = R_{0h}R_{nh}D_1 + D_2 + R_{0h}D_3 + R_{nh}D_4 \tag{3-b}$$

where, R is the reflection coefficient of the wedge type of obstacle. The subscripts s and h are stand for soft (horizontal) and hard (vertical) polarization, respectively. Also the subscripts 0 and n are for zero and n faces of the wedge type of obstacle as shown in Fig. 2, respectively. Polarization is an important issue when obstacles other than edges are considered in diffraction process. Therefore, formulations of diffraction from wedge type obstacles are assessed both for soft and hard polarizations, each of which represents different orientation of electric field vector.

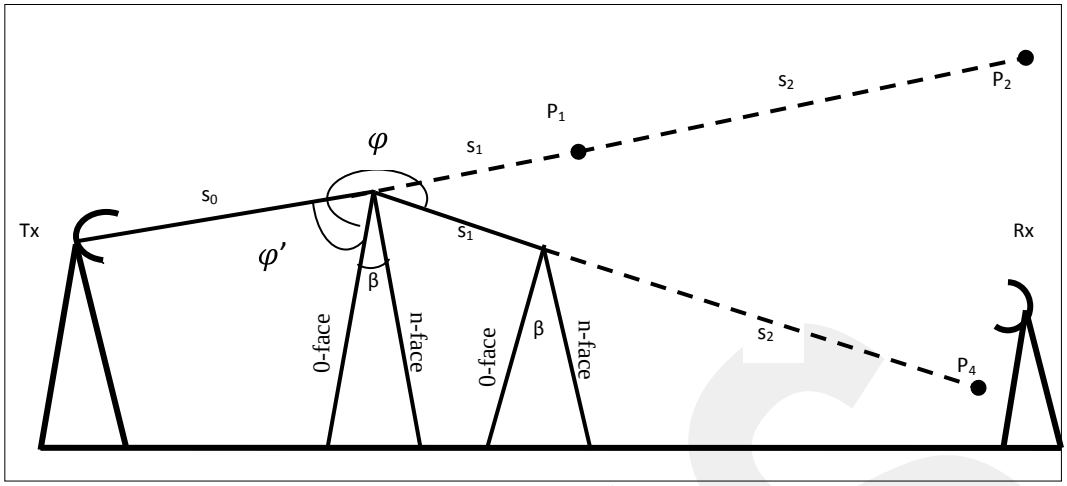

Fig.2. Ray geometry of multiple-diffraction for wedge type of obstacles

D_i is in (3- a, b) is given [20] by

$$D_i = \frac{-e^{-j\pi/4}}{2n\sqrt{2\pi k}} cot(\psi(i))\, F\left(2kLn^2\, sin^2\left(\psi(i)\right)\right) \tag{4}$$

where, $\psi(1)=\frac{\pi+\varphi-\varphi'}{2n}$, $\psi(2)=\frac{\pi-\varphi+\varphi'}{2n}$, $\psi(3)=\frac{\pi-\varphi-\varphi'}{2n}$, $\psi(4)=\frac{\pi+\varphi+\varphi'}{2n}$

and $F\left(2kLn^2\, sin^2\left(\psi(i)\right)\right)$ is the transition function given in Appendix A.

Indices (i=1, 2, 3 and 4) in equation (4) are responsible for backward diffraction, forward diffraction, reflection from *0-face* and reflection from *n-face*. Most of the contribution comes from the forward diffraction.

φ and φ' are angles with respect to the 0-*face* of the obstacle as shown in Fig. 2. Calculation of distance parameters L will be developed later, and the number n in equation (4) is a number related with the interior angle of obstacle, which is given by

$$n = 2 - \beta/\pi \tag{5}$$

where, β is the interior angle of wedge type of obstacle and n changes between the 0 and 2.

In the field strength prediction of wedge type of obstacle, not only diffracted fields, but also reflected fields from the *0* and *n* faces of the wedge type of obstacle have to be taken into account. To calculate the reflected fields, the reflection coefficient for 0 and n faces of obstacle with soft and hard polarization are given [21] by

$$R_{0s} = \frac{\sin(\varphi') - \sqrt{\varepsilon_r - cos^2(\varphi')}}{\sin(\varphi') + \sqrt{\varepsilon_r - cos^2(\varphi')}} \quad (6\text{-a})$$

$$R_{0h} = \frac{\varepsilon_r \sin(\varphi') - \sqrt{\varepsilon_r - cos^2(\varphi')}}{\varepsilon_r \sin(\varphi') + \sqrt{\varepsilon_r - cos^2(\varphi')}} \quad (6\text{-b})$$

$$R_{ns} = \frac{\sin(n\pi - \varphi) - \sqrt{\varepsilon_r - cos^2(n\pi - \varphi)}}{\sin(n\pi - \varphi) + \sqrt{\varepsilon_r - cos^2(n\pi - \varphi)}} \quad (6\text{-c})$$

$$R_{nh} = \frac{\varepsilon_r \sin(n\pi - \varphi) - \sqrt{\varepsilon_r - cos^2(n\pi - \varphi)}}{\varepsilon_r \sin(n\pi - \varphi) + \sqrt{\varepsilon_r - cos^2(n\pi - \varphi)}} \quad (6\text{-d})$$

where, ε_r is the relative permittivity constant of obstacle.

The objective in calculating diffracted field is to estimate field strength due to attenuation caused by diffraction process from the obstacles. From system point of view, the corresponding metric is path loss. Path loss is a measure of the average RF attenuation suffered by a transmitted signal when it arrives at the receiver, after traversing a path of several wavelengths. Relative path loss is that path loss divided by free space loss. Relative path loss is calculated by,

$$RPL_{dB} = 10 \log PL/FL \quad (7)$$

where, *PL* and *FL* are path loss and free space loss given by,

$$PL = [E_i D] A(s) e^{-jks} \text{ and } FL = \left[\frac{E_0}{s}\right] e^{-jkr}$$

where, *r* is the LOS distance between the transmitter and receiver.

Excess loss, another parameter used for comparison of model, is the difference between the relative path losses of the models.

After introducing the formulas for the wedge type of obstacle with soft and hard polarization, the amplitude diffraction coefficient for knife-edge type of obstacle as shown in Fig. 3 is given [8] by,

$$D(\alpha) = -\frac{e^{-j\pi/4}}{2\sqrt{2\pi k\cos(\alpha/2)}}F[x] \tag{8}$$

where $\alpha \equiv \varphi - \varphi'$ and $x = 2kL\cos^2(\alpha/2)$.

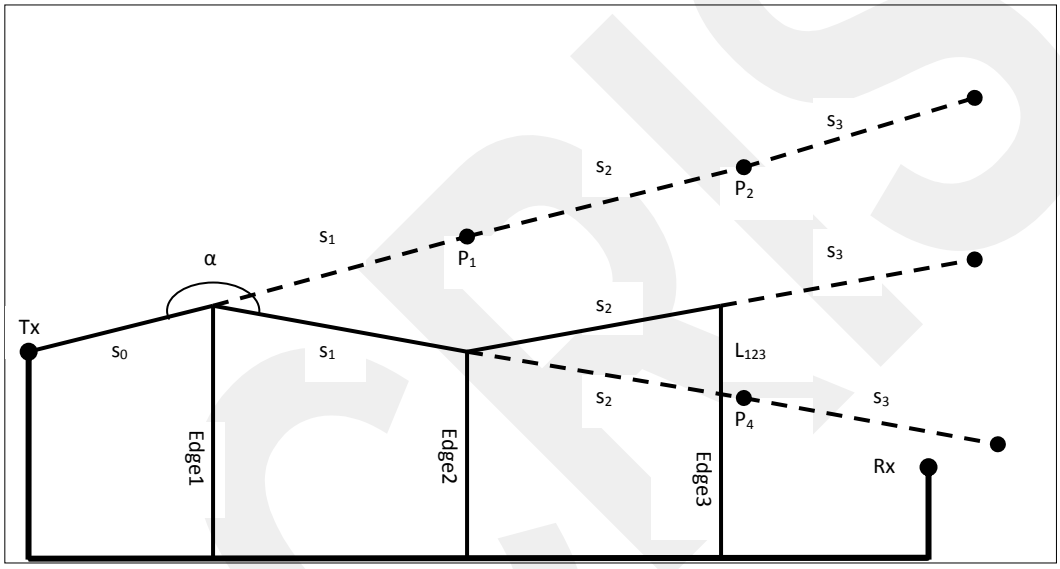

Fig.3. Ray geometry of multiple knife edge diffraction

Uniform Theory of Diffraction (UTD) model has been used for a long time. In case that even if one obstacle is in the transition zone of the previous, UTD fails to predict the relative path loss accurately in multiple diffraction geometries. That is, UTD gives huge discontinuities in the transition zone in case of multiple diffracting geometries. UTD predictions are in good agreement with exact solution in case that the geometry including one obstacle or in case that obstacle is not in the transition region of previous obstacle(s). To prove this assertion following test case taken from [6] is studied. The propagation path is 10 km, the operational frequency is 100 MHz and transmitter height is 50 m. Receiver height changes from -100 to 200 m. A single knife-edge or wedge type of obstacle of 50 m with 160° interior angle is placed at distance 5 km from the

transmitter. There are 3 simulations in Fig. 4. Solid line represents single knife edge type of obstacle. The dashed and the dotted lines is represents single wedge type of obstacle with hard and soft polarization, respectively. As the interior angle of the obstacle reduces to zero, the geometry is simplified to the knife-edge type of obstacle problem.

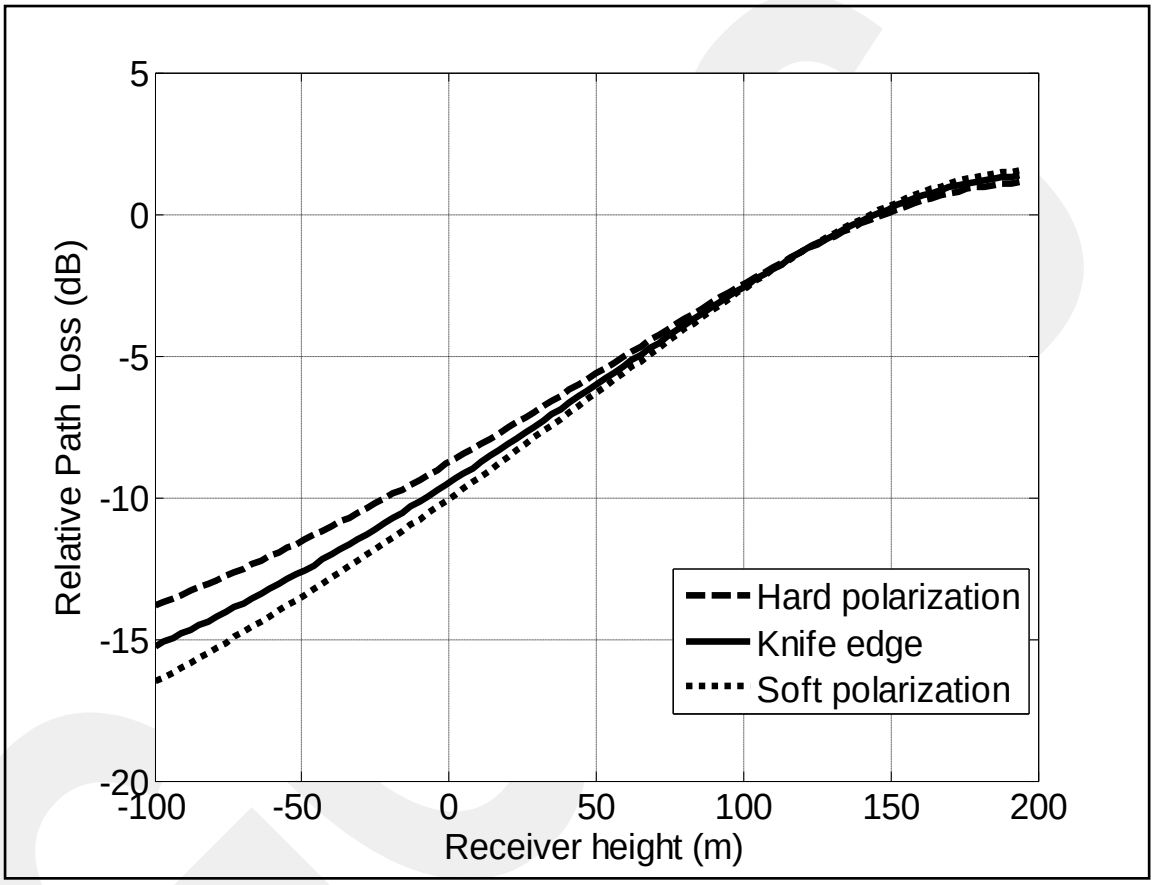

Fig. 4 Relative path loss versus receiver height for knife edge and wedge types of obstacle

When using wedge type of obstacles not only heights of obstacle, but also interior angle, relative permittivity constant and conductivity of obstacle affects the path loss profile. It can be seen [16, Figs. 3 and 4], relative path loss decreases due to increasing interior angle and relative permittivity constant of obstacle. In addition to this, conductivity of obstacle is another parameter affecting the relative path loss at the receiver. Relative path loss increases as conductivity of obstacle decreases.

Up to this point only single knife-edge or wedge type of obstacle has been taken into account. It is seen from the simulations that UTD predicts the field strength accurately for single diffraction. If the number of diffraction increases, UTD fails to predict the field strength accurately. From this point, some simulations are made to show that even if one obstacle is in the transition zone of the previous obstacle, UTD gives huge discontinuities in that zone. To show that, UTD fails to predict the field accurately for multiple diffraction in the transition region, the following test case taken from [6-8] is studied. The propagation path is 18 km, the operational frequency is 100 MHz and transmitter height is 40 m. Receiver height changes from -200 to 200 m. There are two knife-edge or wedge type of obstacles height of 50 and 40 m at a distance of 8 and 10 km interior angle of obstacle is 60º. In Fig. 5, there are three simulations showing the relative path loss versus receiver height for this double diffraction. The dashed line indicates double diffraction for knife-edge type of obstacle. The solid and dotted lines indicate double diffraction for wedge type of obstacle with hard and soft polarizations, respectively. As can be seen from Fig. 5, there is discontinuity in the relative path loss up to 3 dB due to that placing the second edge in the transition region of first edge.

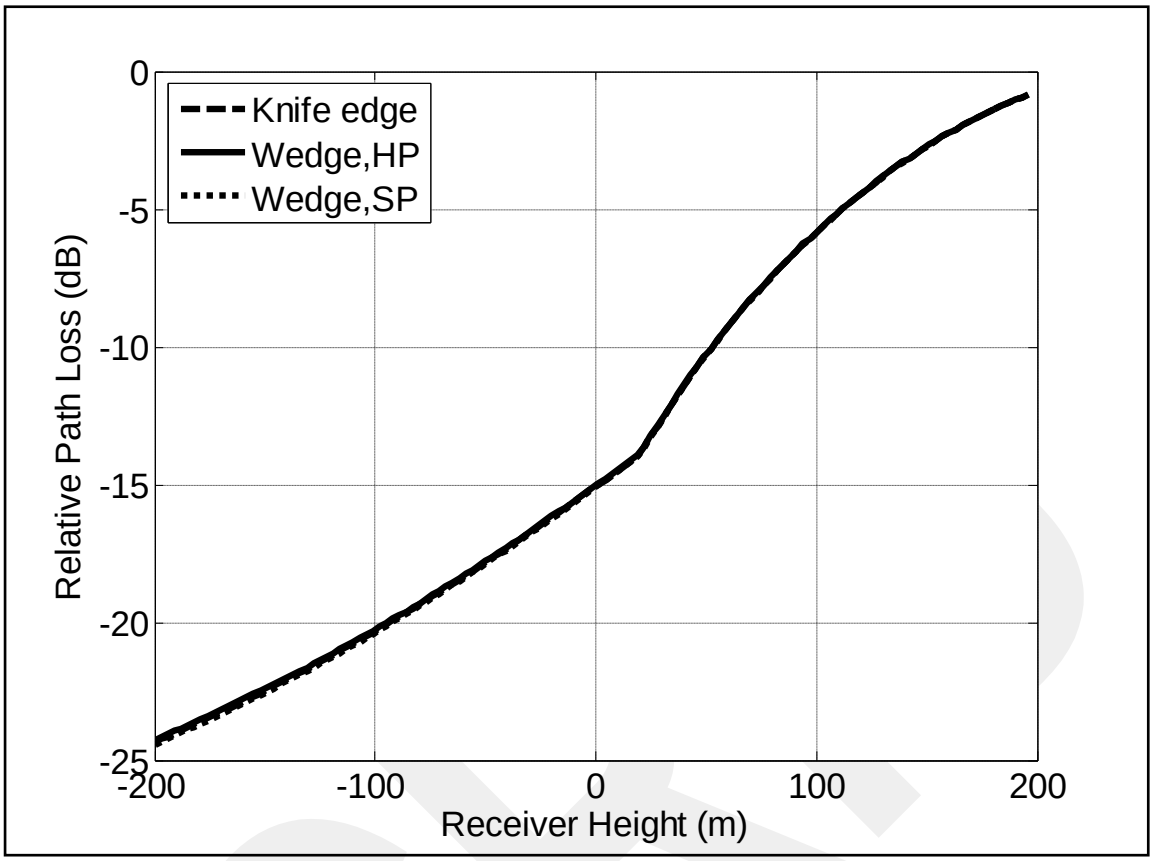

Fig. 5 Relative path loss versus changing receiver height for double knife edge and double wedge types of obstacle with hard and soft polarization

Another test case to show UTD model's failure in multiple transition zone diffraction is taken from [5-9]. The propagation path is 30 km, the operational frequency is 100 MHz and transmitter and receiver heights are 0 m. Second knife edge or wedge type of obstacle with 30° interior angle height changes from -200 to 600 m at a distance 15 km. There are two knife edges or wedges types of obstacle with 30° interior angle and heights of 100 m are at a distance of 10 and 20 km. Fig. 6 shows the relative path loss predicted by UTD model versus receiver height for the triple diffractions for knife-edge or wedge types of obstacle. In this figure, there are three simulations for knife edge and wedge type of obstacle with hard and soft polarizations. As can be seen from Figs. 6 and 10, there are huge discontinuities in relative path loss at the transition zone due to that obstacles are in the transition zone of the first and second obstacle. Also it can be

concluded from the figure, UTD model refers to the first order expansion of the model [6].

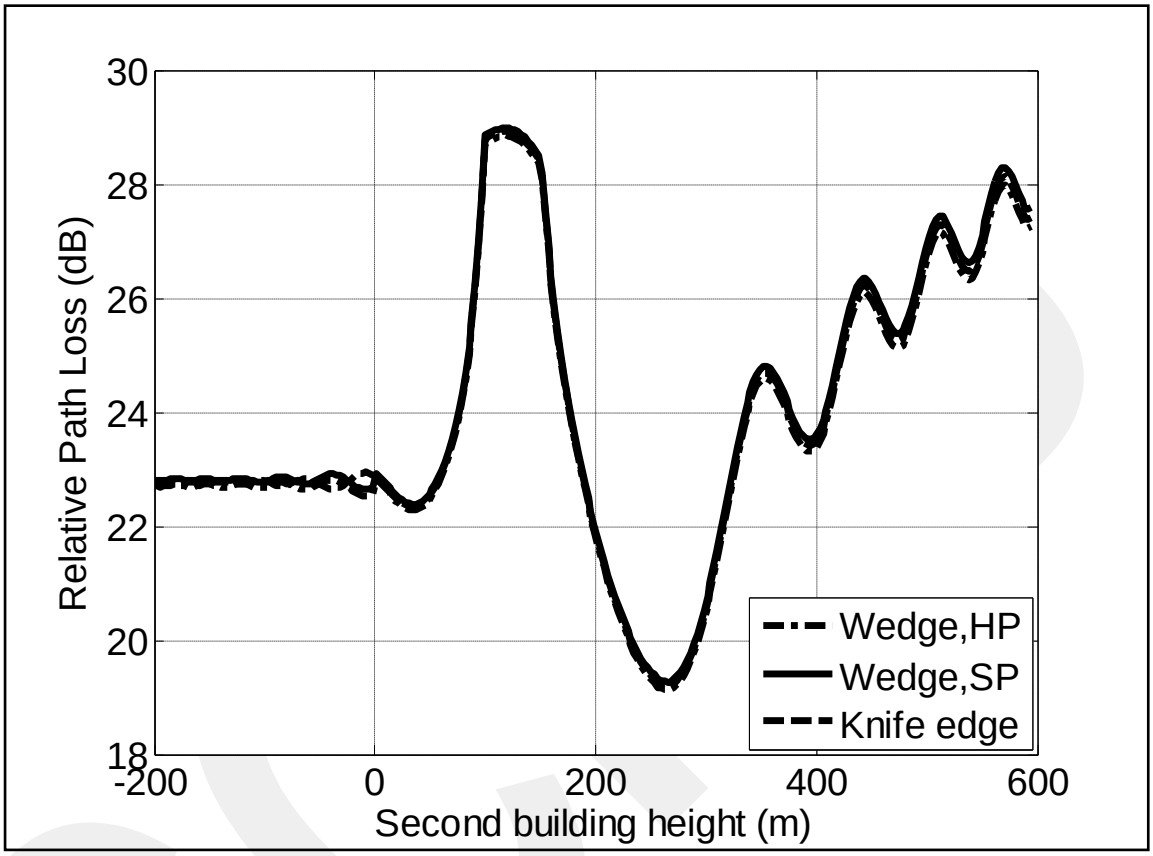

Fig. 6 Relative path loss versus changing receiver height for triple knife edge and triple wedge types of obstacle with hard and soft polarization

Obstacles can be treated as knife edge or wedge type of obstacle for UHF applications [1]. The propagation path is 18 km, the operational frequency is 100 MHz and transmitter height is 0 m, and receiver height changes from 0 to 300 m. There are eight wedge types of obstacle with 1° interior angle and heights of 10, 40, 60, 30, 20, 25, 45 and 10 m are at a distance from 2, 4, 6, 8, 10, 12, 14, and 16 km, respectively. Relative permittivity constant of the obstacles are 5. Fig. 7 shows the relative path loss versus receiver height for the scenario including eight wedge types of obstacles.

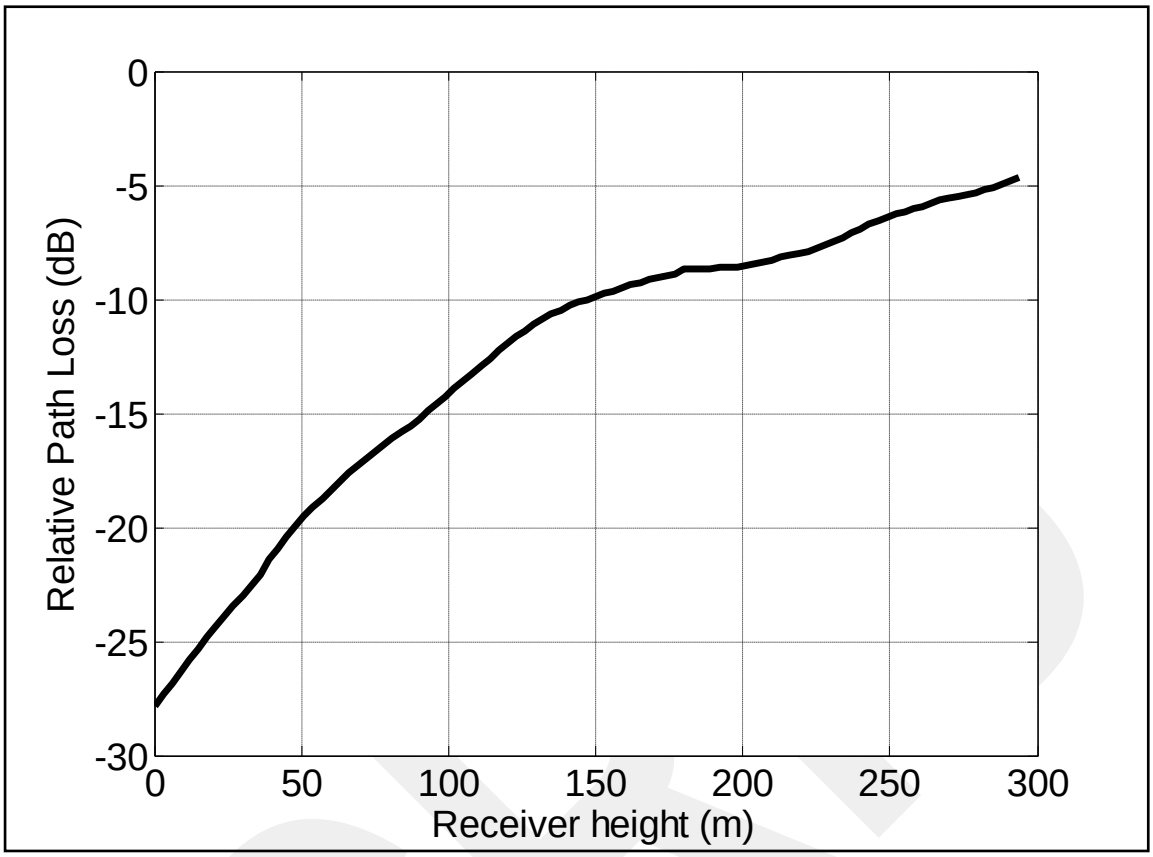

Fig. 7 Relative path loss profile for 8 wedge type of obstacle for broadcasting system

CHAPTER 3

HIGHER ORDER DIFFRACTED FIELDS

In this chapter, discontinuities appearing at the transition zone are removed via using higher order diffracted fields. Although adding higher order diffracted fields to total field increase the accuracy, it increases the computation complexity, too. Instead of using higher order terms, in this chapter only first order diffracted is used for heuristic model, which is called slope UTD (S-UTD). S-UTD model [5], removes most of the discontinuities in the transition zone. Extensive information and simulation results are given to show that S-UTD removes most of the discontinuities in this chapter.

According to UTD formulation [25], field of doubly diffracted ray as shown in Fig. 8 is given by,

$$E_{UTD} = \frac{E_0}{s_1} e^{-jks_T} \sqrt{\frac{s_T}{s_1 s_2 s_3}} \sum_{m=0}^{\infty} \frac{1}{m!} \left(\frac{-1}{jks_2}\right)^m \frac{\partial^m D_1}{\partial \varphi_1^m} \frac{\partial^m D_2}{\partial \varphi_2^{'m} \partial \varphi_2^i} \tag{9}$$

where, s_1, s_2 and s_3 are the distance between the obstacles as shown in Fig. 8. s_T is the total distance between the transmitter and receiver. E_0 is the incident field. m is the order of diffraction. φ' and φ are the angles as shown in Fig. 8. The case $m = 0$ refers to classical UTD [2]. Distance parameters (L_1 and L_2) calculated analytically for diffraction coefficient are given [26] by

$$L_1 = \frac{s_1 s_2}{(s_1 + s_2)} \text{ and } L_2 = \frac{(s_1 + s_2) s_3}{(s_1 + s_2 + s_3)}$$

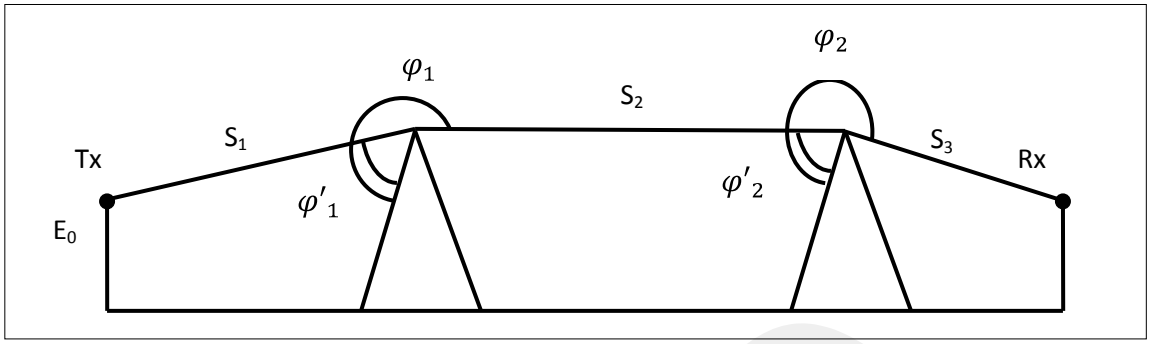

Fig.8 Ray geometry for diffraction by two wedge types of obstacles

Instead of the using the equation (9) which requires extensive computations, only first order derivatives along with heuristic approach in [5] can be used. $m = 1$ in the equation (9) can be used with the same accuracy as given [27, 28] by

$$E = \left[E_i D + \frac{\partial E_i}{\partial n} d_s\right] A(s) e^{-jks} \tag{10}$$

where, $E_i D$ and $\frac{\partial E_i}{\partial n} d_s$ refer to zero and first order (classical UTD and S-UTD) terms of the equation (9). d_s is the slope diffraction coefficient given [8] by

$$d_s(\alpha) = \frac{1}{jk} \frac{\partial D(\alpha)}{\partial \alpha} . \tag{11}$$

where, Slope diffraction coefficients ds_s and ds_h for soft and hard polarizations derived from (11) are given [20] by

$$ds_s = \frac{\partial R_{0s}}{\partial \varphi'} R_{ns} D_1 + R_{0s} R_{ns} \frac{\partial D_1}{\partial \varphi'} + \frac{\partial D_2}{\partial \varphi'} + \frac{\partial R_{0s}}{\partial \varphi'} D_3 + R_{0s} \frac{\partial D_3}{\partial \varphi'} + R_{ns} \frac{\partial D_4}{\partial \varphi'} \tag{12-a}$$

$$ds_h = \frac{\partial R_{0h}}{\partial \varphi'} R_{nh} D_1 + R_{0h} R_{nh} \frac{\partial D_1}{\partial \varphi'} + \frac{\partial D_2}{\partial \varphi'} + \frac{\partial R_{0h}}{\partial \varphi'} D_3 + R_{0h} \frac{\partial D_3}{\partial \varphi'} + R_{nh} \frac{\partial D_4}{\partial \varphi'} \tag{12-b}$$

Derivative of the reflection coefficient with respect to φ' is given by

$$\frac{\partial R_{0s}}{\partial \varphi'} = \frac{2\cos(\varphi')(\varepsilon_r - 1)}{\sqrt{\varepsilon_r - cos^2(\varphi')}\left(\sin(\varphi') + \sqrt{\varepsilon_r - cos^2(\varphi')}\right)^2} \tag{13-a}$$

$$\frac{\partial R_{0h}}{\partial \varphi'} = \frac{2\varepsilon_r \cos(\varphi')(\varepsilon_r - 1)}{\sqrt{\varepsilon_r - cos^2(\varphi')}\left(\sin(\varphi') + \sqrt{\varepsilon_r - cos^2(\varphi')}\right)^2} \tag{13-b}$$

$$\frac{\partial R_{ns}}{\partial \varphi'} \text{ and } \frac{\partial R_{nh}}{\partial \varphi'} = 0 \tag{13-c}$$

Derivative of D_i with respect to φ' is given by

$$\frac{\partial D_i}{\partial \varphi'} = \frac{-e^{-j\pi/4}}{2n\sqrt{2\pi k}} \left(\frac{\partial \cot(\psi_i)}{\partial \varphi'} F_{x_i} + \cot(\psi_i) \frac{\partial F_{x_i}}{\partial \varphi'} \right) \tag{14}$$

where, $\frac{\partial \cot(\psi_i)}{\partial \varphi'} = \pm \frac{\csc \psi_i{}^2}{2n}$ for $i = 1$ and 3 the minus sign shall be taken into account, whereas for $i = 2$ and 4 the plus one. Moreover, $\frac{\partial F_{x_i}}{\partial \varphi'}$ is derivative of the transition function as detailed in appendix A.

When the number of obstacle is greater than 2 derivative of the slope diffraction coefficient for hard and soft polarization have to be calculated.

$$\frac{\partial ds_s}{\partial n} = \frac{1}{s}\left[\begin{array}{c} \frac{\partial^2 R_{0s}}{\partial \varphi'^2} R_{ns} D_1 + 2\frac{\partial R_{0s}}{\partial \varphi'} R_{ns} \frac{\partial D_1}{\partial \varphi'} + R_{0s} R_{ns} \frac{\partial^2 D_1}{\partial \varphi'^2} + \frac{\partial^2 D_2}{\partial \varphi'^2} + \\ \frac{\partial^2 R_{0s}}{\partial \varphi'^2} D_3 + 2\frac{\partial R_{0s}}{\partial \varphi'} \frac{\partial D_3}{\partial \varphi'} + R_{ns} \frac{\partial^2 D_4}{\partial \varphi'^2} \end{array}\right] \tag{15-a}$$

$$\frac{\partial ds_h}{\partial n} = \frac{1}{s}\left[\begin{array}{c} \frac{\partial^2 R_{0h}}{\partial \varphi'^2} R_{nh} D_1 + 2\frac{\partial R_{0h}}{\partial \varphi'} R_{nh} \frac{\partial D_1}{\partial \varphi'} + R_{0s} R_{nh} \frac{\partial^2 D_1}{\partial \varphi'^2} + \frac{\partial^2 D_2}{\partial \varphi'^2} \\ + \frac{\partial^2 R_{0h}}{\partial \varphi'^2} D_3 + 2\frac{\partial R_{0h}}{\partial \varphi'} \frac{\partial D_3}{\partial \varphi'} + R_{nh} \frac{\partial^2 D_4}{\partial \varphi'^2} \end{array}\right] \tag{15-b}$$

Derivations of all parameters in equation (15- a, b) are provided in appendix C.

After introducing the formulas for the wedge type of obstacle for soft and hard polarizations, the slope diffraction coefficient for the knife edge type of obstacle is given [5, 7 and 8] by

$$d_s(\alpha) = -\frac{e^{-j\pi/4}}{\sqrt{2\pi k}} L_s \sin(\alpha/2)\big(1 - F(x)\big) \tag{16}$$

And its normal derivative is given by

$$\frac{\partial d_s(\alpha)}{\partial n} = \frac{1}{s}\frac{dd_s}{d\alpha} =$$

$$-\frac{1}{2s}\frac{e^{-j\pi/4}}{\sqrt{2\pi k}}\left\{L_s \cos(\alpha/2)[1 - F(x)] + 4L_s^2 k sin^2(\alpha/2)\cos(\alpha/2)\, F'(x)\right\}. \tag{17}$$

S-UTD [5] proposed that adding first order diffracted field to total field removes the most of the discontinuities at the transition region. To prove this idea the geometry given in chapter 2 is re-considered in here. As can be seen from Fig. 9, by applying first order term, the discontinuity is removed by adding slope diffraction terms.

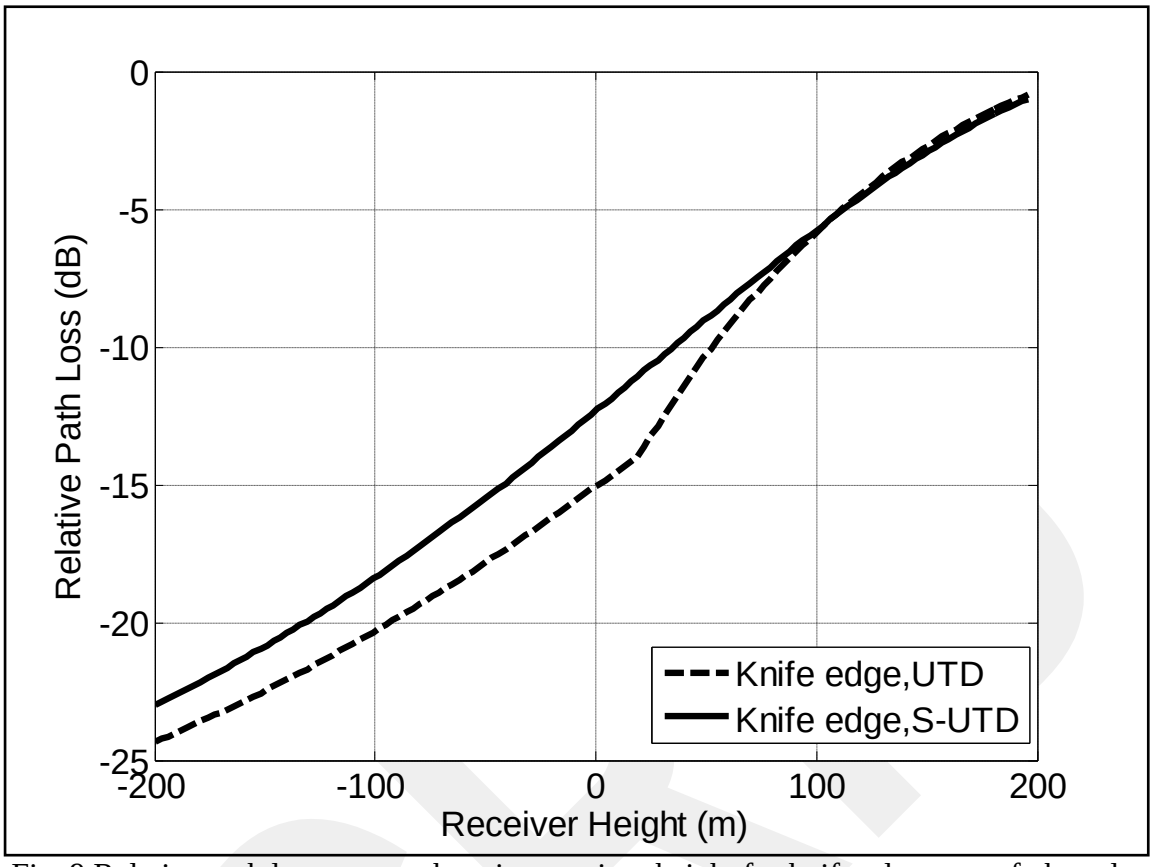

Fig. 9 Relative path loss versus changing receiver height for knife edge type of obstacle

Although S-UTD [5] removed most of the discontinuity in the transition zone, there are still discontinuities at the shadow boundary points as seen in Figs. 2 and 3 for the wedge and knife-edge type of obstacle. Discontinuities at the shadow boundary points results from the fact that phase continuity in calculating the distance parameters are not taken into consideration. To solve that problem an improvement to slope UTD [7, 8] is proposed with imposing the amplitude, slope and the phase continuities in calculation of the distance parameters for amplitude and slope diffraction coefficients as described in appendix B.

A test case is provided in [6-9] to illustrate the contribution of phase continuity. The frequency is 100 MHz, the distance between antennas is 30 km, and at 10, 15 and 20 km there are three knife edge types of obstacles. Transmitter and receiver antennas height is zero. First and third obstacle height is 100 m. Second edge height varies from -200 to 600 m. As previously mentioned, imposing the phase continuity in calculation of the

distance parameter removes the discontinuity at the shadow boundary points as shown in Fig. 10. It can also be seen from the figure, as the second edge height is greater than 300 m models give the same results due to that edges are not in the transition region of the previous one.

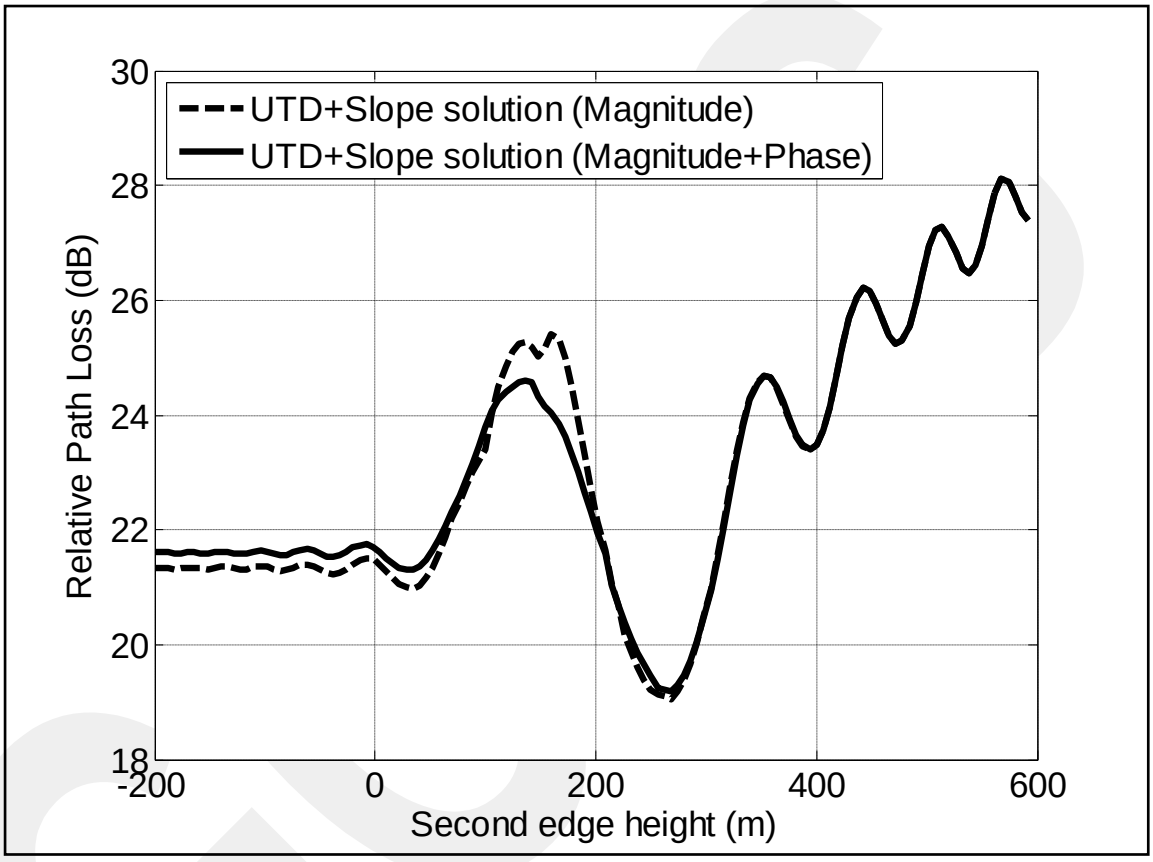

Fig. 10 Improvement in Slope UTD by adding phase continuity

To show contribution of phase continuity in calculation of distance parameters, a test case taken from [6, 29] is performed and the simulation results are given [17, Figs. 4 and 5]. A few more tests were considered and improvement in the model has been validated in [6]. It can be seen from this figures; S-UTD model with imposing phase continuity is in good agreement with higher order diffracted field model [6].

To prove that S-UTD [7, 8] gives the same results with numerical model [9] known with ultimate accuracy, the classical test case of [9] was also considered here, and results are presented in the following. The propagation path is 50 km, the operational frequency is 500 MHz and transmitter height is zero. Receiver height changes from 300 to 650 m. A single fixed knife edge type of obstacle with a height of 420 m is at a distance of 42 km from the transmitter. Fig. 11 shows the relative path loss versus receiver height. Also it shows that as diffraction number increase, the relative path loss increase. In Fig. 11 there are 3 different conditions of the path.

i) two additional knife edges types of obstacle, evenly spaced between 0 and 42 km, for a total of three obstacles,

ii) four additional knife edge type of obstacle, evenly spaced between 0 and 42 km, for a total of five obstacles,

iii) six additional knife edge type of obstacle, evenly spaced between 0 and 42 km, for a total of seven obstacles.

In all cases the heights of the additional obstacles are such that the tops just graze the direct line between the transmitter and the obstacle at 42 km.

It can be seen from Fig. 11, heuristic approach S-UTD [7, 8] agrees exceptionally well with the exact solution [9, 25] with lower computation time.

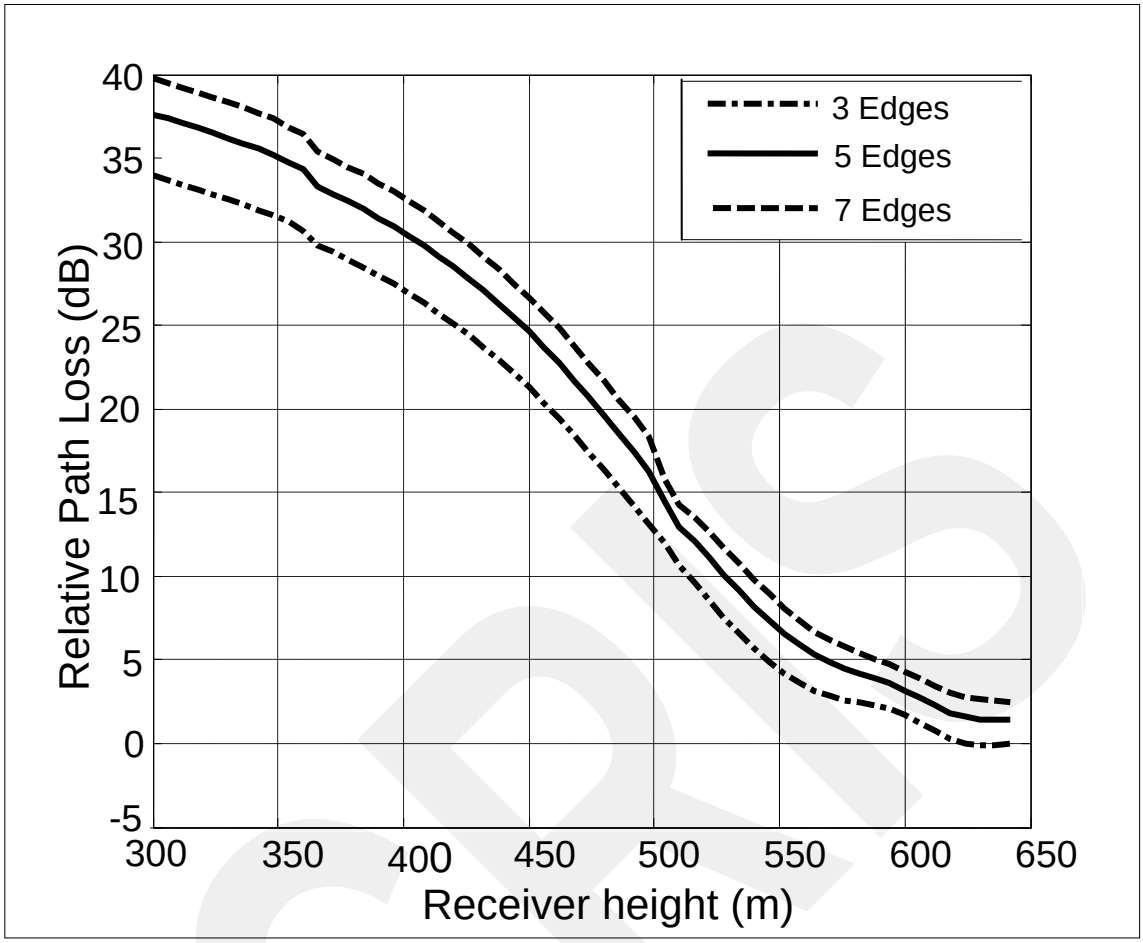

Fig. 11 Relative path loss versus changing receiver height

So far, it has been proved that S-UTD [7, 8] gives approximately the same results with numerical solution [9] and higher order diffracted field model [6]. From this point, 2 test cases are studied for greater number of obstacle with various geometries. These test cases are performed to show the S-UTD contribution in the transition zone. The first test scenario for multiple-diffraction is given in Fig. 12. The propagation path is 400 m, the operational frequency is 900 MHz and transmitter and receiver height is 0. In that case interior angle of wedge type of obstacle is approximately zero and obstacles are distributed with equal distances and also the top of the obstacle is lying on a parabola as shown in Fig. 12. Even if one obstacle is in the transition region of the previous, Classical UTD fails to predict the relative path loss accurately.

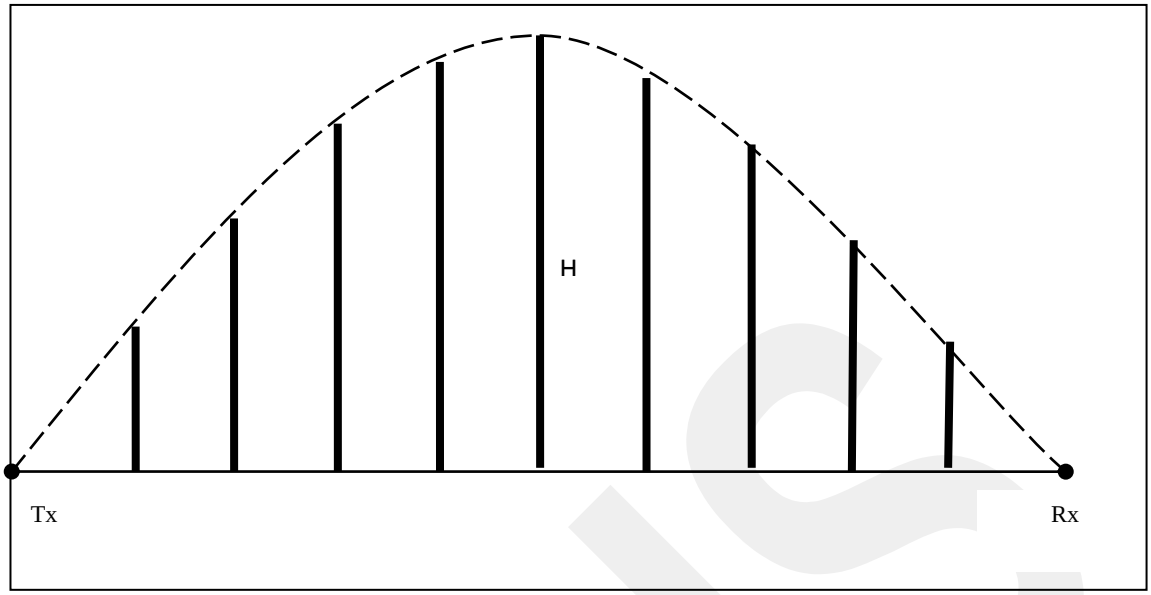

Fig. 12 Test scenario for contribution of the S-UTD model (convex case)

Table 1 shows the contribution of the S-UTD to total relative path loss at the receiver as the obstacles are in the transition region of the previous obstacles. It can be seen in Table 1, first column shows the y-axis of the vertex. Next 2 columns show the computation time for S-UTD and UTD. The last column shows the contribution of S-UTD to UTD. It can be concluded from the Table 1, as H decreases, obstacle heights become nearly the same and obstacles enter the transition zone of the previous one. In that case, UTD fails to predict the path loss accurately.

Table 1 Contribution of the S-UTD to total relative path loss at the receiver (convex)

H(m)	Time (s) /S-UTD	Time (s) /UTD	Contribution (dB)
3	679	31	24,5
2	719	31	25,4
1	715	31	26,4
0,5	689	31	26,9
0,1	688	30	27,3
0,01	670	29	27,4
0	2366	23	37

The second test scenario for the multiple-diffraction is given in Fig. 13. The propagation path is 400 m, the operational frequency is 900 MHz and transmitter and receiver height is H m. In that case interior angle of the wedge type of obstacle is approximately zero and obstacles are distributed with equal distances and also the top of the obstacles lying on a parabola as shown in Fig. 13. Even if one obstacle is in the transition region of the previous, Classical UTD fails to predict the relative path loss accurately.

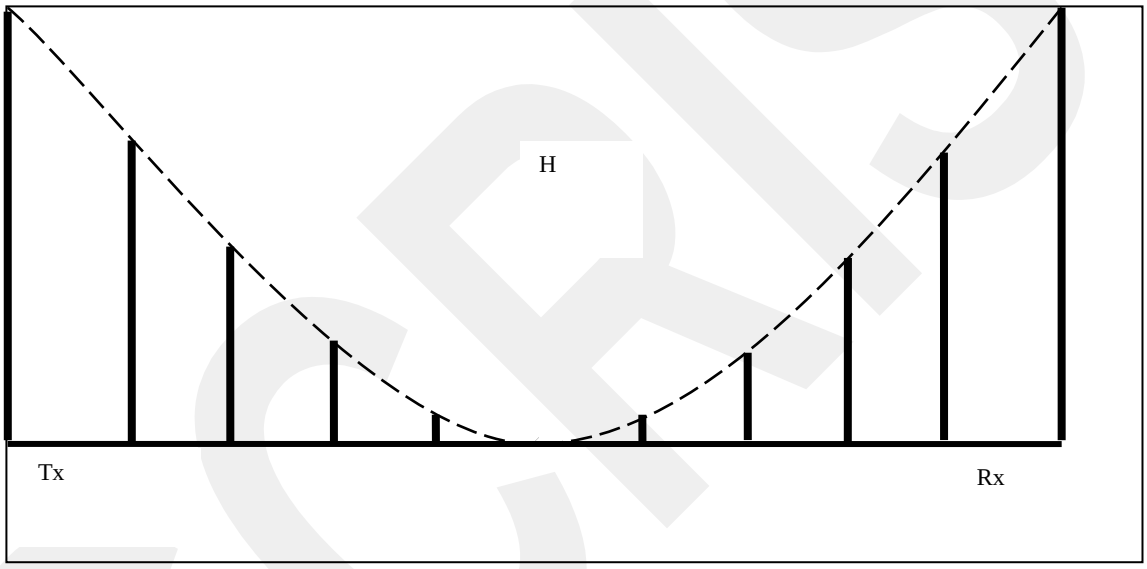

Fig. 13 Test scenario for contribution of the S-UTD model (concave case)

Table 2 shows the contribution of the S-UTD to total relative path loss at the receiver as the obstacles are in the transition region of the previous. It can be seen in Table 2, first column shows the y-axis of the vertex. Next 2 columns show the computation time for S-UTD and UTD. The last column shows the contribution of S-UTD to UTD. Moreover it can be say about the Table 2, as the H decreases, UTD fails to predict the path loss accurately.

Table 2 Contribution of the S-UTD to total relative path loss at the receiver

H(m)	Time (s) /S-UTD	Time (s) /UTD	Contribution (dB)
3	2839	31	0,4
2	3585	31	0,4
1	2859	31	4
0,5	2833	31	9
0,1	2832	30	21
0,01	2803	29	33
0	2366	23	37

S-UTD model gives excellent agreement with higher order diffracted fields model [6] and Vogler's [9] model up to 9-10 diffractions. After 9-10 diffractions S-UTD loses the accuracy and requires more computation time. S-UTD model cannot be used for the geometry including large number of obstacles. In that case S-UTD-CH model can be used for more accurate results with relatively lower computation time.

CHAPTER 4

SLOPE UTD WITH CONVEX HULL

In this chapter, a new approach that combines S_UTD with convex hull is presented. This provides an improvement to S-UTD implementation both for computation time and accuracy when the number of obstacles (or diffraction) in transition region is large (usually greater than 9 or 10). For multiple edges with various geometries, it is necessary to develop a ray tracing code to include all ray variations to the field strength at the receiver. Therefore, a ray tracing algorithm is developed, and is presented in this chapter. Then Fresnel zone and construction of the convex hull is explained. Finally, S-UTD-CH algorithm is explained. Extensive simulations are performed to show that S-UTD-CH gives the same results with relatively lower computation time. Moreover, S-UTD-CH model can be used in broadcasting applications.

4. 1. Ray Tracing Algorithm

Ray tracing is widely used in conjunction with UTD methods when multiple diffraction edges or wedges are considered. The algorithm developed here runs in two ways. One is that all the abscissa and ordinate of obstacles can be entered manually. The other is that obstacles coordinates can be distributed randomly. The algorithm is described on a simple geometry as shown in Fig. 14. The distance between antennas is 10 km, and at 4, 6 and 8 km there are three obstacles in 40, 50 and 60 m heights. Firstly LOS case is inspected via the equation given by,

$$y = (x - T_x)\left(\frac{R_y - T_y}{R_x - T_x}\right) + T_y \tag{18}$$

where, T_x and T_y are the abscissa and ordinate of the transmitter, R_x and R_y are the abscissa and ordinate of the receiver, x and y are the abscissa and ordinate of the line anywhere we want to find.

Abscissa of obstacle, transmitter and receiver coordinates are entered into the equation (18) and ordinate of the line in that point is calculated. If this point is greater than obstacles ordinate there is no intersection. In other words, there is no obstacle blocked the line between two points. This process continues until all obstacles are inspected.

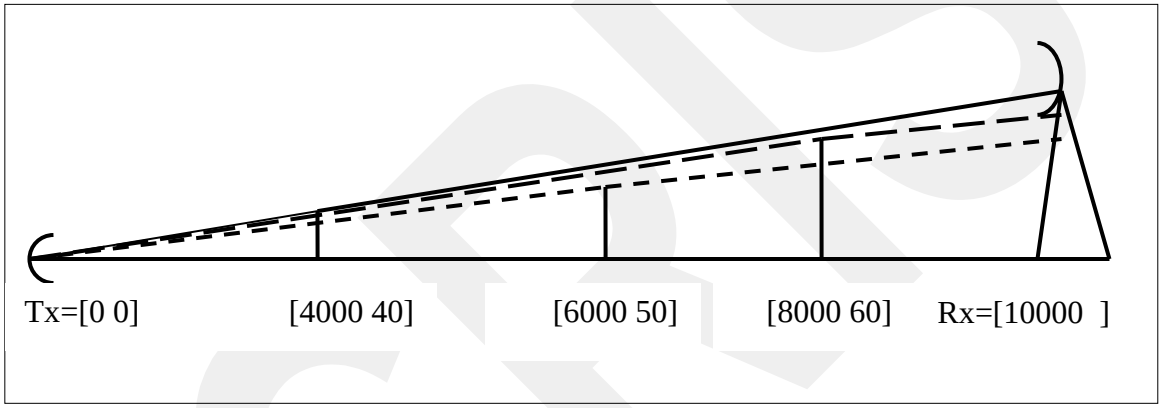

Fig. 14 Ray tracing scenario

As can be seen in Fig. 14, there is no path (0, 2...) due to that it is blocked by the first obstacle.

Finally, all ray paths contributing to total field are found: (0 1 4), (0 1 3 4), (0 1 2 3 4)

Ray tracing algorithm can be explained on another scenario in the Fig. 15. There is 30 km between the transmitter and receiver and heights of the transmitter and receiver are 40 and 60 m. There are 7 knife edge types of obstacle whose heights are 50, 30, 100, 70, 120, 0, 20, 170, -30 m at a distance from the receiver antenna 4, 6, 8, 10, 12, 15, 17, 20 and 26 km as shown in Fig. 15.

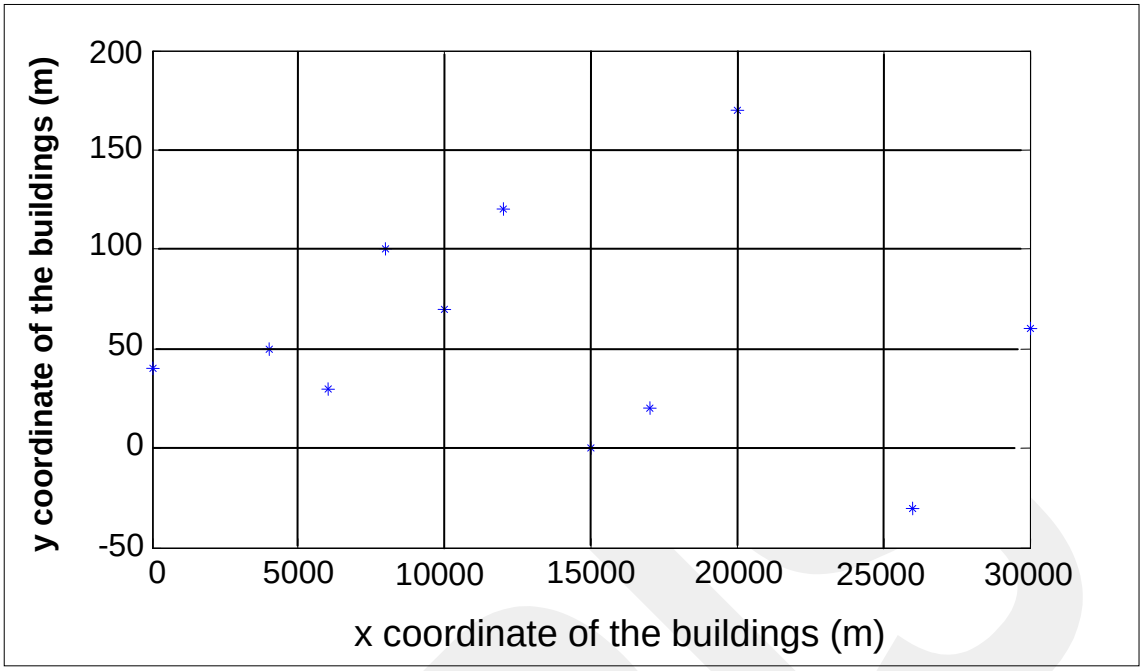

Fig. 15 Ray tracing test scenario

After ray tracing algorithm runs, some of ray paths are obtained as follows in Table 3.

Table 3 Some of the ray paths for the given geometry

0	0	0	0	0	0	0	0	0	0	0	0	0	0	0	0	0	0
1	1	1	1	1	1	1	1	1	1	1	1	1	1	1	1	1	1
2	2	2	2	2	2	2	2	2	2	2	2	2	2	2	2	2	2
3	3	3	3	3	3	3	3	3	3	3	3	3	3	3	3	3	3
4	4	4	4	4	4	4	4	5	5	5	5	5	5	5	5	8	8
5	5	5	5	5	5	5	5	6	6	6	6	7	7	8	8	9	10
6	6	6	6	7	7	8	8	7	7	8	8	8	8	9	10	10	
7	7	8	8	8	8	9	10	8	8	9	10	9	10	10			
8	8	9	10	9	10	10		9	10	10		10					
9	10	10		10				10									
10																	

As can be seen from the Table 3, each column shows different ray path. For example the first column shows the ray originating from the transmitter and diffracted from all edges and arriving at the receiver. For the given scenario there are totally 54 ray paths.

Computation time for determining the ray path is 0.3 seconds. As the number of the knife edges increases, elapsed time increases exponentially. Since it is 2D geometry, the computation time is not so much, and most practical scenarios to be considered in this thesis requires not more than 3 seconds in MATLAB. All the subsequent simulations and theory is based on the use of the ray tracing algorithm developed here.

4. 2. Fresnel Zones

Fresnel zone concept widely been used in radio propagation modeling in urban/suburban and rural areas. Fresnel zones are concentric ellipsoid of revolution about the direct line from a transmitter to a receiving point, with the transmitter and receiving points serving as foci of the ellipse [29] as shown in Fig. 16.

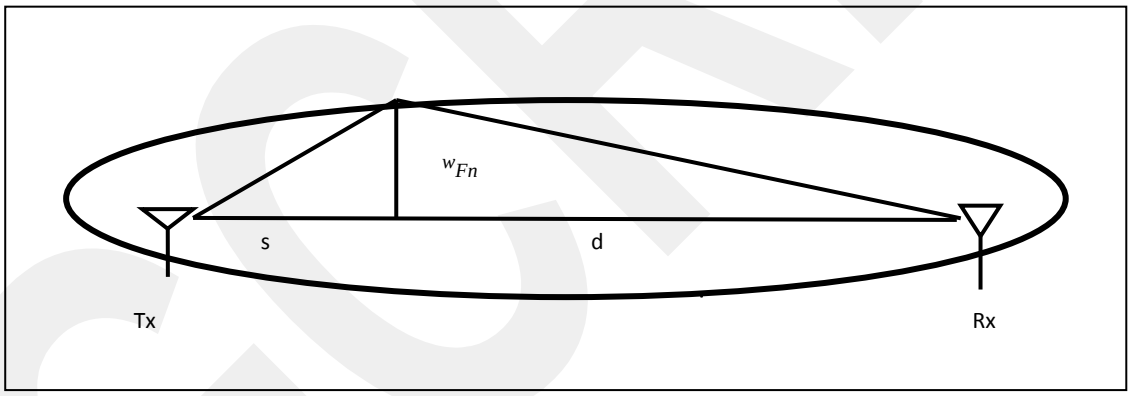

Fig. 16 Fresnel zone

w_{Fn} is radius of nth Fresnel zone at a given distance given [22] by

$$W_{F_n} = \sqrt{m\frac{\lambda sd}{s+d}} \tag{19}$$

where, m is the order of the Fresnel zone and λ is the wavelength of the incoming electromagnetic wave.

Fresnel zone radius is the maximum at the midpoint between the transmitter and receiver. As the frequency of the electromagnetic wave increases, the radius of the Fresnel zone decreases. Moreover, Fresnel zone radius decreases as the distance between the transmitter and receiver increases. Most of the fields propagate in this zone. It can be concluded that if there is no disruption of the Fresnel zone, total path loss almost does not change. In other words, obstacles are outside of the Fresnel zone; do not disturb the path loss profile of the geometry. For that reason these obstacles can be ignored [13-18]. On the contrary, if there is disruption by the ground or an obstacle, total path loss profile changes. Some disruptions of the Fresnel zone are shown in Fig. 17. Not only direct path, but also diffracted or reflected rays from the obstacle have to be taken into account.

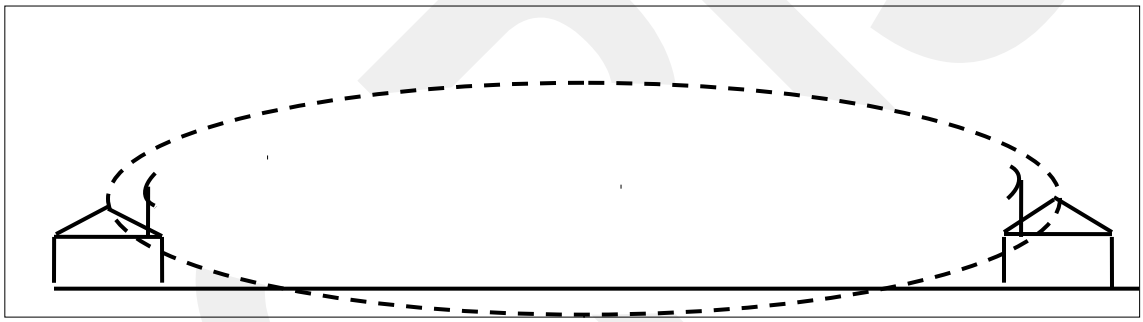

(a) Disruption by the ground

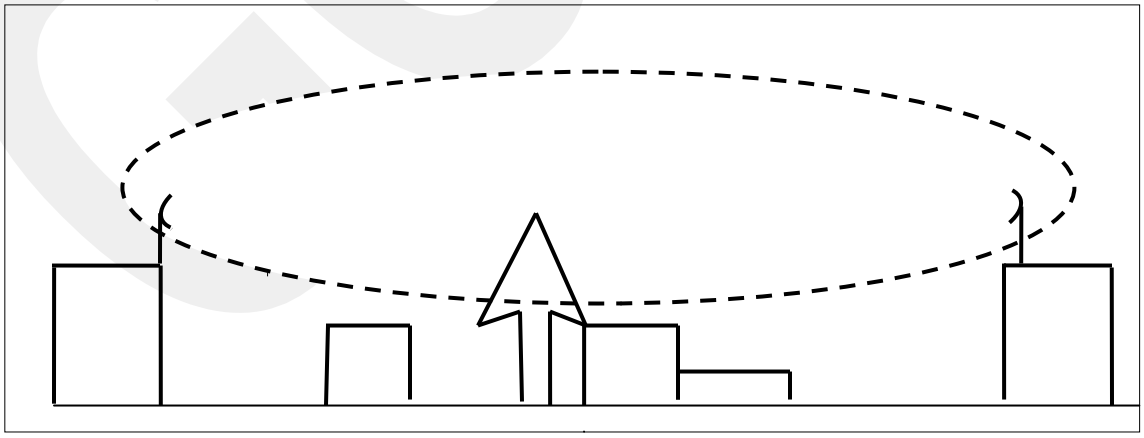

(b) Disruption by an obstacle

Fig. 17 Disruption by (a) ground, (b) (obstacle)

4. 3 Convex Hull Method

Convex hull is described as a polygon formed by some selected obstacles between the transmitter and receiver positions [30]. Convex hull method based on Fresnel zone concept. Via convex hull method, some obstacles having almost no contribution to the total path loss are eliminated. This elimination results faster algorithm to predict the path loss at the receiving point. Convex hull algorithm runs as follow. For a given obstacle height distribution, firstly, the main Fresnel zone is constructed between the transmitter and the receiver, and obstacles outside the main Fresnel Zone are eliminated. Then, the highest obstacle intersecting the line between the transmitter and receiver is selected. If there is no such line, elimination is completed. Next, the secondary Fresnel zones are constructed between the transmitter and the highest obstacle, and then the highest obstacle and the receiver. Again, obstacles outside these secondary Fresnel zones are eliminated. The process is repeated successively for smaller Fresnel zone to be constructed under the secondary Fresnel zones until no obstacles are remained for elimination as shown in Fig. 18.

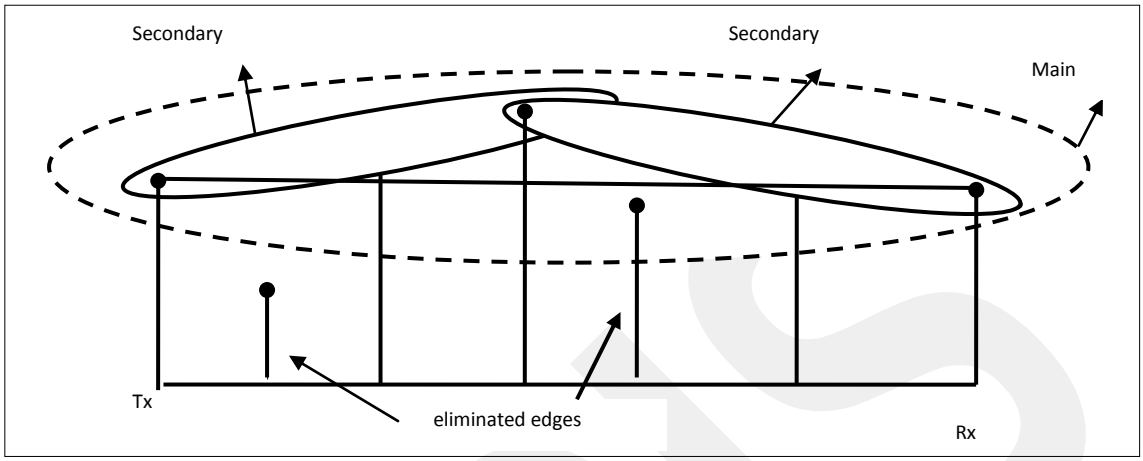

(a)

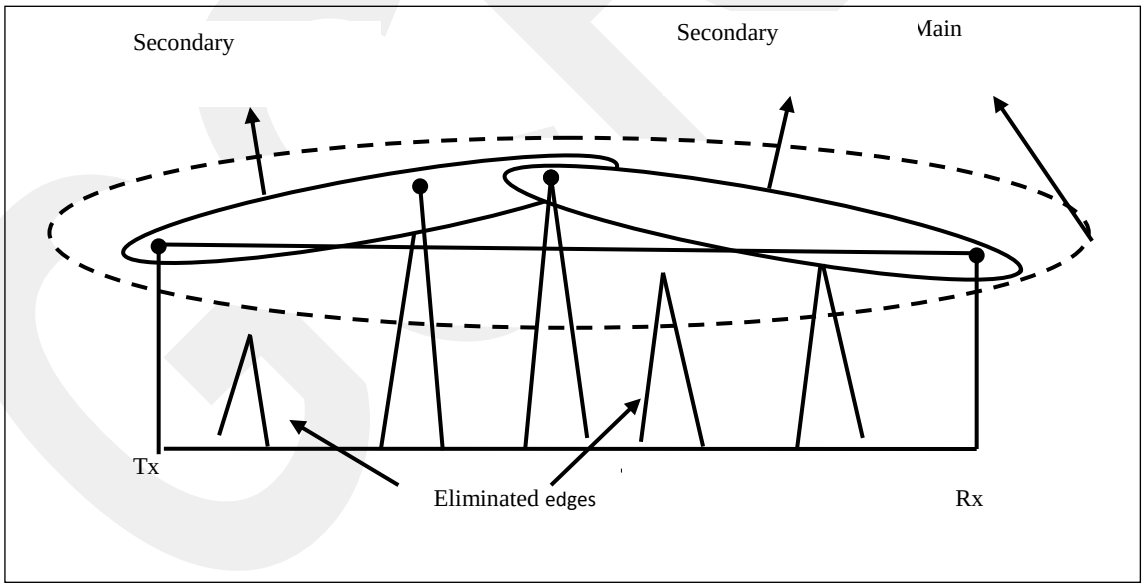

(b)

Fig. 18 Elimination for (a) knife-edge type obstacle, (b) wedge type of obstacle

From mathematical point of view convex hull constructed as follows: Firstly, main Fresnel zone is constructed between the transmitter and receiver whose tips are the foci of the ellipsoid. Then a direct line is drawn between the transmitter and receiver antennas' tips. Next, the highest diffracting obstacle intersecting the line between the antennas is determined via controlling all the diffracting obstacles.

The equation of the line can be found by the formula is given in (18), d_x and d_y are the abscissa and ordinate of the diffracting obstacle,

- If $y - w_{F_n}/\cos(a) < d_y$, diffracting obstacle is eliminated.
- If $d_y < y$, elimination process is completed.

Finally, the convex hull is constructed as shown in Fig. 19 by the remained obstacles as a result of the elimination process.

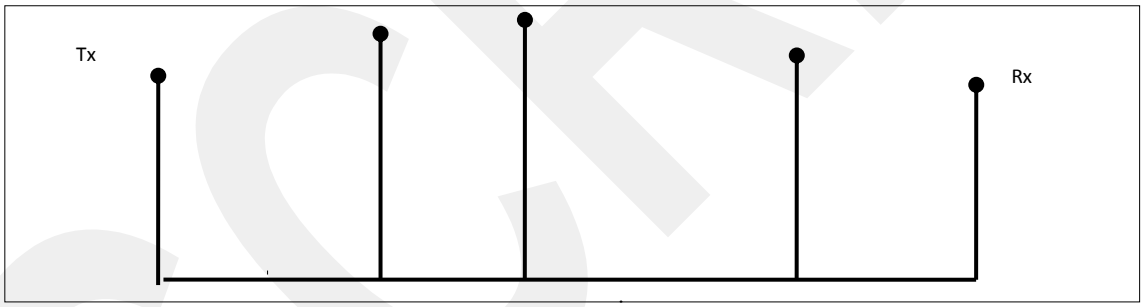

(a)

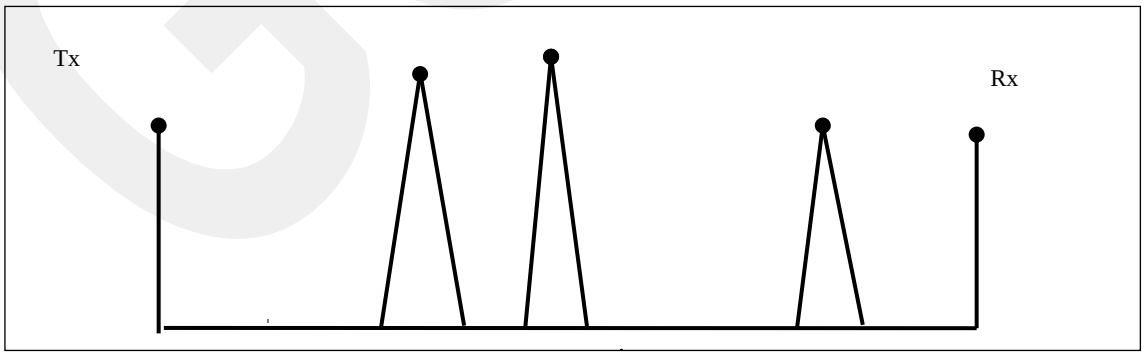

(b)

Fig. 19 Convex hull construction for (a) knife edge type of obstacle, (b) wedge type of obstacle

The motivation for this approach of eliminating less important obstacles was to reduce both computation time and make a compromise between computation time and error when the number of diffractions is large.

4. 4. Slope UTD with Convex Hull Algorithm

From theoretical point of view, the diffraction from obstacles placed outside the first Fresnel zone does not contribute much to the received field, and can be ignored for most cases. After forming the convex hull, 2D ray tracing algorithm described in section 4.1 runs to find all the rays originated from the transmitter to the receiver point. Finally, S-UTD algorithm runs for calculating the total field at the receiver. Contribution of this approach is that less important obstacles are eliminated to reduce both computation time and error of S-UTD model for the geometry having many obstacles.

In implementation of slope UTD, although obstacles placed outside Fresnel zone generate new rays, these rays have only small effect on dominant rays generated by obstacles placed inside first Fresnel zone. When obstacles placed outside Fresnel zone can be determined and be eliminated before running slope UTD, then the computation time can be substantially reduced with minimum error. Eliminating one obstacle approximately decreases the computational time one-fifth, and the less obstacles are left in the Fresnel zone, the less the computational time.

To show the process following test case is considered in Fig. 20 (a). The obstacles are of knife-edge type in the Fig. 20 (a). The frequency is 100 MHz, the distance between the antennas is 20 km, and at 5, 10 and 15 km there are three knife edge type of obstacle of 100, h2, and 100 m heights, respectively. Receiver height varies in between -300 to 400 m. When the second obstacle is placed outside the Fresnel zone, the diffraction effects of 3 obstacles turns out to be effect of 2 obstacles, i.e., 3 obstacles can be represented by 2 obstacles in terms of contribution to the received field as shown in Fig. 20 (b).

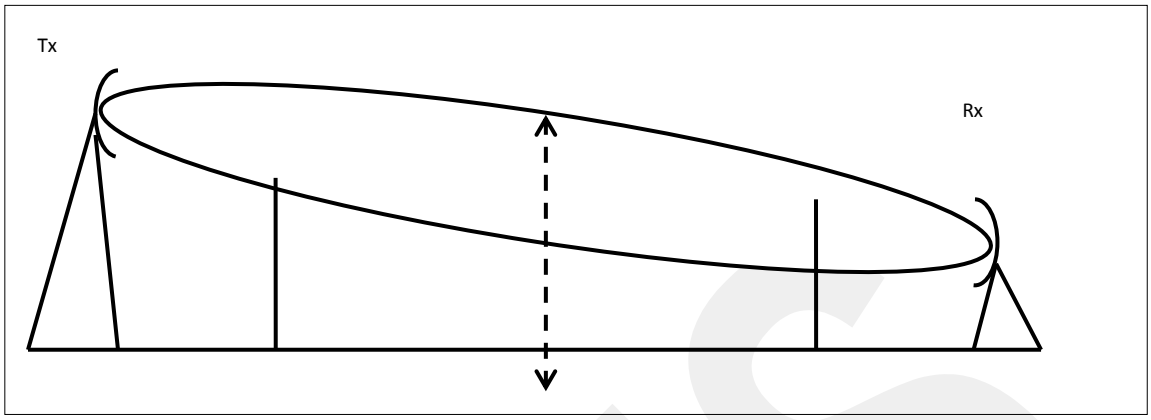

Fig. 20 (a) The Fresnel zone for 3 knife edge types of obstacle

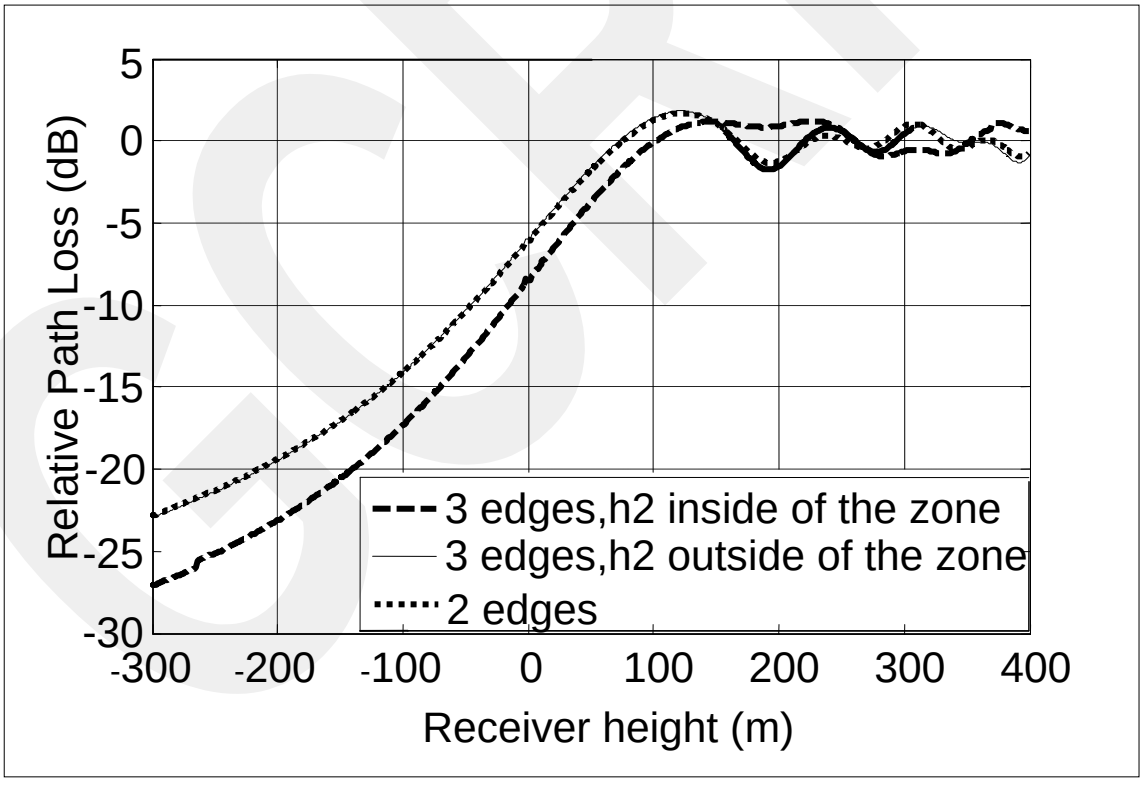

Fig. 20 (b) Relative path loss for 3 (and 2) knife edge types of obstacle

This can also be proved for the wedge type of obstacle. As test case shown in Fig. 21 (a) is studied for proving that the obstacles are placed outside the Fresnel zone can be ignored because of having small contribution to the total field strength. The frequency is 100 MHz, the distance between antennas is 20 km, and at 5, 10 and 15 km there are three wedge type of obstacles of h1, 40, and 60 m heights, respectively. Interior angles of obstacles are 60°. Receiver height varies in between -300 to 300 m. When the first obstacle is placed outside the Fresnel zone, the diffraction effects of 3 obstacles turns out to be effect of 2 obstacles, i.e., 3 obstacles can be approximated by 2 obstacles in terms of contribution to the received field as shown in Fig. 21 (b).

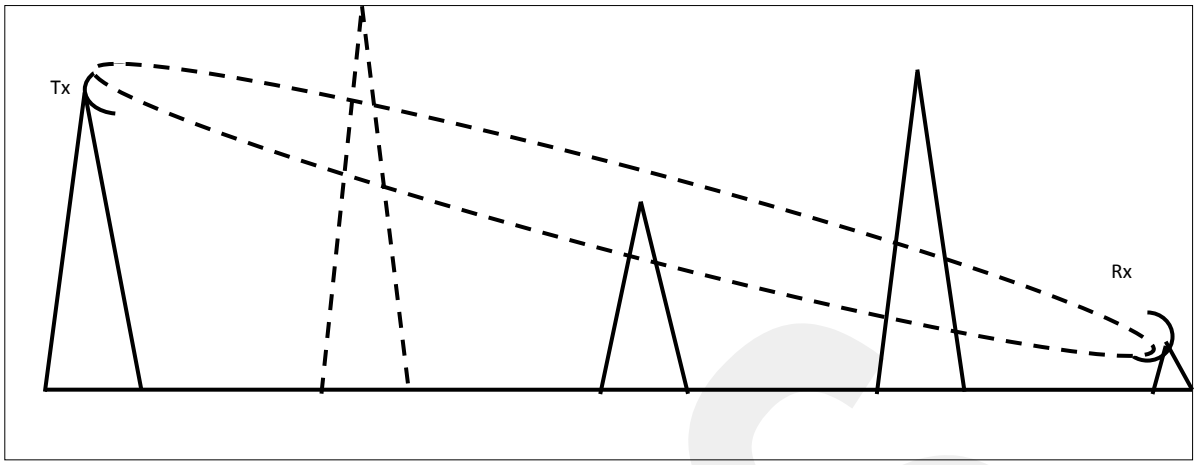

Fig. 21 (a) The Fresnel zone for 3 wedge types of obstacles

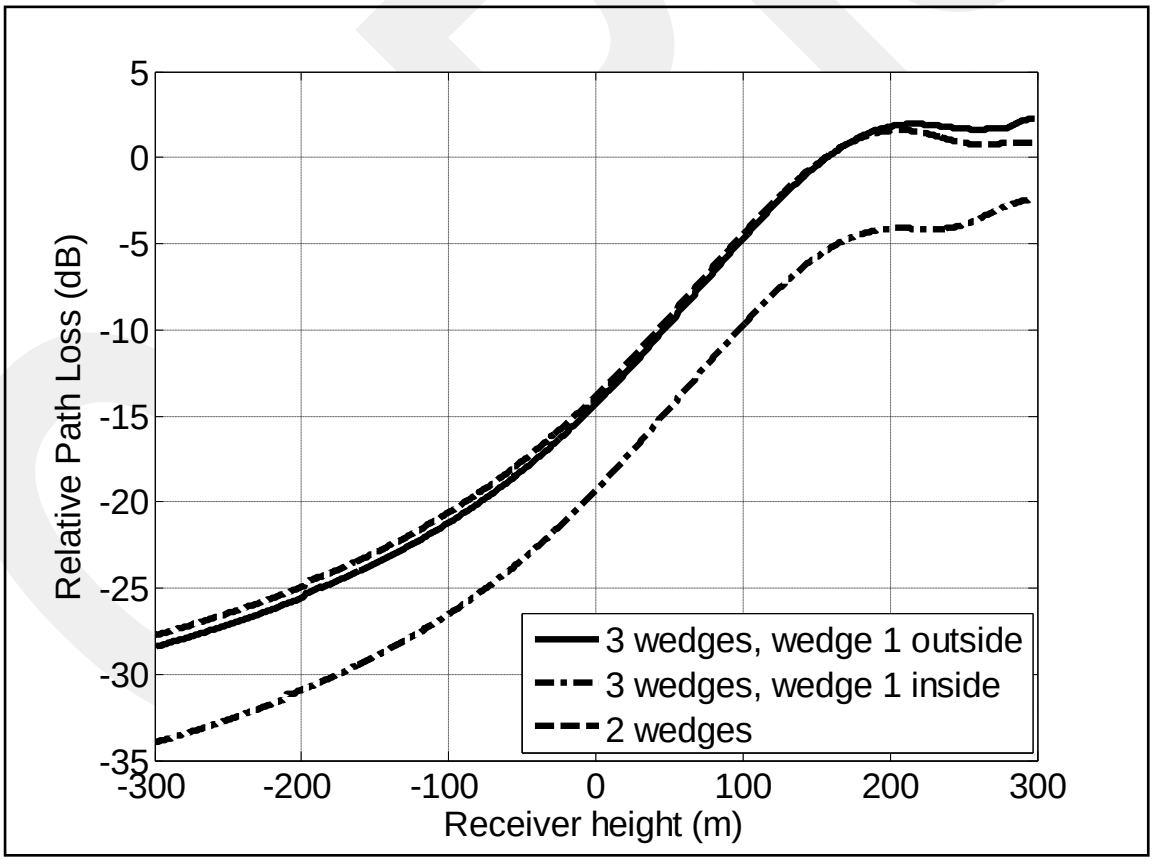

Fig. 21 (b) Relative path loss for 3 (and 2) wedge type of obstacles

After introducing the S-UTD-CH model, comparison of UTD based models (UTD, S-UTD, S-UTD-CH) is given. To compare the models double wedge scenario given in chapter 2 is studied with relatively higher frequency (1800 MHz). In that case soft polarization is considered and the results are given in Fig. 22. There are 3 models considered here: UTD, S-UTD and S-UTD-CH. As can be seen from the figure, S-UTD and S-UTD-CH gives almost the same results. However UTD model gives relatively higher error resulted from the fact that the second obstacle is in the transition zone of the previous one. One can say that there is only 1 dB difference between the soft and hard polarization as shown in [16, Fig10].

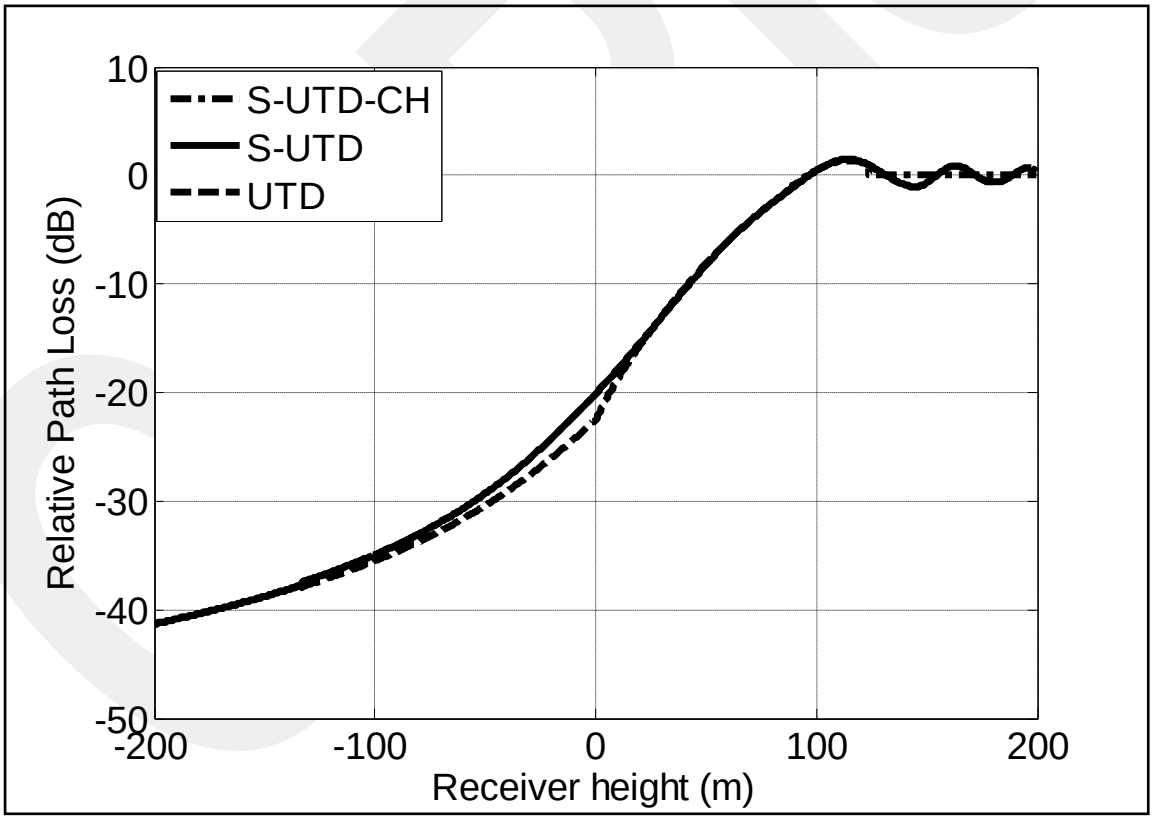

Fig. 22 Comparison of UTD based models with soft polarization

S-UTD-CH model can also be used for prediction of coverage in broadcasting systems. In the case that obstacles like hills, mountains and high-rise buildings have relatively higher variations in heights, UTD model can be used with accurate predictions. On the other hand, when the variation in heights is not so large, corresponding to approximately equal height case (transition zone), UTD model cannot be used for field prediction. Then, S-UTD would be good option for accurate prediction of field strength. However, as the number of diffractions increases, computation time of S-UTD model increases and model loses accuracy. Instead of using that model, S-UTD-CH model have to be used for accuracy and its computation time.

As an example following test case is considered. The transmitter height is 80 m, the operational frequency is 400 MHz, and receiver height changes between 0 and 120 m. There are 7 hills as obstacles with 60º interior angle. At 6, 14, 20, 25, 30, 36, 45 and 50 km there are seven obstacles of 100, 30, 70, 25, 80, 60 and 40 m heights, respectively. Simulation results are given in Fig. 23 with hard polarization. There are 3 conditions in simulation for UTD, S-UTD and S-UTD-CH models. As can be seen from the figure S-UTD and S-UTD-CH gives almost the same results. However UTD model gives relatively higher error resulted from that obstacles are in the transition zone of the previous.

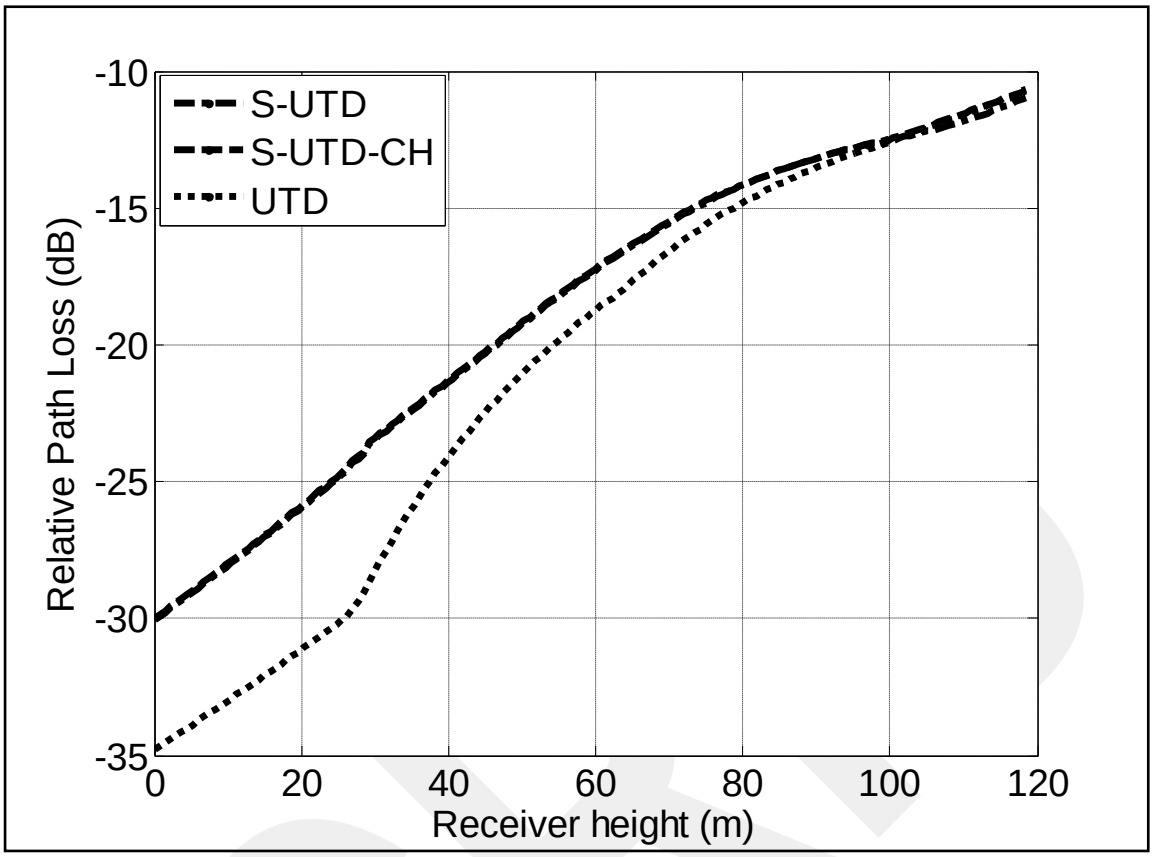

Fig. 23 Relative path loss calculation for broadcasting systems

Moreover Table 4 gives the elapsed time for the given geometry. As can be seen, UTD is the fastest solution with relatively higher error in field prediction. S-UTD-CH model is optimum solution with respect to its computation time and good agreement with S-UTD model for the field strength. S-UTD-CH gives almost the same results with S-UTD with lower computation time due to eliminating the unimportant diffracting obstacles.

Table 4 Computation times for UTD based models

Computation Time (s) UTD	Computation Time (s) S-UTD	Computation Time (s) S-UTD-CH
119	5068	1201

CHAPTER 5

STATISTICAL COMPARISON OF MODELS

In this chapter extensive comparison results are given for more obstacles including geometry. In all simulations, obstacles are considered as knife edge. Firstly, UTD based models compared with each other. Then UTD based models compared with a numerical PO model. Finally S-UTD-CH model compared with numerical PO model.

5. 1 Comparison of UTD Based Models

In this section there are two different types of scenarios; the first one is for equal spacing, the other is for unequal spacing case.

5. 1. 1. Knife-edges distributed with equal spacing

To compare accuracy of ray theoretic models UTD, S-UTD and S-UTD-CH, a particular multiple-edge geometry having 9 equally spaced knife-edges is considered as shown in Fig. 24.

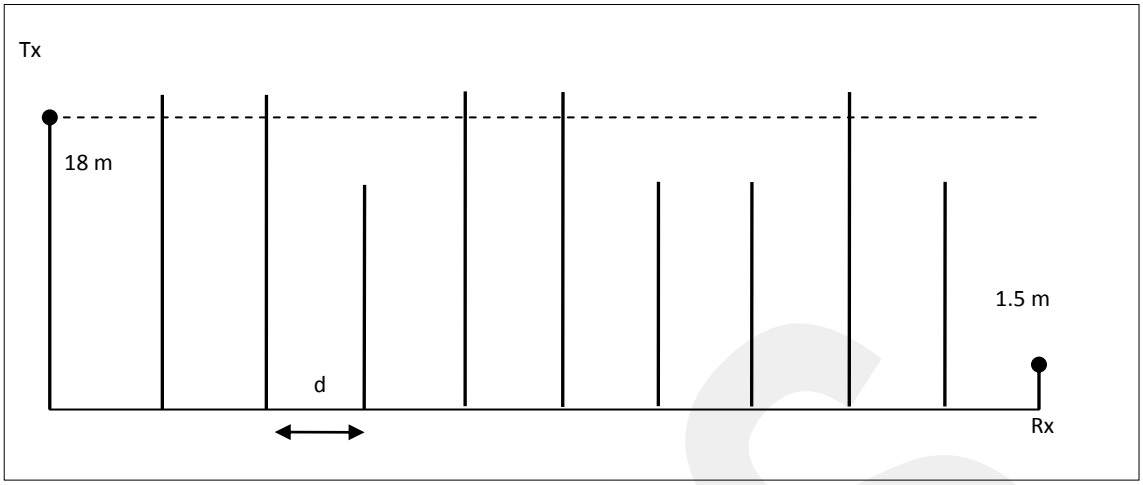

Fig. 24 Equally spaced screens with heights distributed according to a uniform distribution: U [18-Δh, 18+Δh] m

All simulations are conducted in the following parameter ranges that might represent a canonical multiple edge transition zone diffraction geometry as reported in [7]:

Difference between the heights (Δh) =1, 3 and 6

Distance between the edges (d): 25 and 50m

Operating frequency (f): 0.9 GHz, 1.8 GHz and 2.1 GHz

Instead of analyzing contributions of each parameter range to the field strength prediction or accuracy, a combined parameter called transition region width in [7] is used in simulations is given by

$$\frac{2s_0 s_1 \cos\frac{\varphi-\varphi'}{2}}{\lambda(s_0+s_1)} \leq 1 \tag{20}$$

where, For $d >> \Delta h$, the angle α as shown in Fig. 3 is approach to zero and the equation (20) is simplified to transition region width (TRW) calculated [7] via

$$TRW \cong \frac{\Delta h^2}{\lambda d}. \tag{21}$$

Some TRW values for the geometries given above are given in Table 5. As can be seen from the table, there are three values in each cell. The first ones is TRW value for the

frequency of 0.9 GHz. The values in parenthesis are TRW for the frequency of 1.8 GHz. And the last values in curly brackets are TRW for the frequency of 2.1 GHz.

Table 5 Transition Region Width (TRW) for several values for the frequencies of 0.9, 1.8, 2.1 GHz.

Δh(m) / d(m)	1	3	6
25	0.12, (0.24), {0.28}	1.08, (2.16), {2.52}	4.32, (8.64), {10.08}
50	0.06, (0.12), {0.14}	0.54, (1.08), {1.26}	2.16, (4.32), {5.04}

Algorithms for UTD, S-UTD and S-UTD-CH have been developed in MATLAB environment, and simulations were performed to cover all parameter ranges listed above. Table 6 shows the mean (μ) and standard deviation (σ) of error for excess loss predicted by UTD and S-UTD-CH assuming that S-UTD is the most accurate one.

All parameter ranges listed above can be represented by some TRW values calculated from (21). In Table 6, the rightmost column represents "average" number of ignored/eliminated edges by S-UTD-CH model (for each run, actually this is an integer number out of 9 edges). Average computation time of each model including S-UTD is also presented in Table 7.

In simulations, there were 10 runs for each model at each TRW value, and mean error (μ) and standard deviation (σ) values of error are calculated accordingly. In all model implementation, phase summing of ray fields is used.

First, UTD and S-UTD can be compared for accuracy. Then, S-UTD and S-UTD-CH can be compared for computation time. For multiple transition zone diffraction for TRW=0.2 or lower, while UTD is faster (~5 s) and simpler to implement than S-UTD (~1100s), it is not as accurate as S-UTD (>4 dB mean error). Therefore, S-UTD-CH can be used in some TRW ranges (TRW>1). For example, S-UTD-CH predicts field strength as accurate as S-UTD for TRW>0.5 with relatively smaller computation time (179 s vs.

1133 s). In such cases, eliminating one edge might reduce computation time pretty much due to the complexity of slope diffraction algorithm itself. However, S-UTD-CH has no advantage for very small TRW values (<0.5) where there is no edge that can be ignored. For TRW>3 values, UTD might be satisfactory for accurate prediction if small error can be tolerated.

Although TRW value is used to represent combinations of geometrical (distances) and system (frequency) parameters, the effect of individual parameters could also be compared via the variation of TRW values. For fixed Δh and d parameters, the operational frequency can vary, and this is still corresponding to a variation in TRW. However, the range of frequency and geometrical parameter of the problem should be consistent to have practical meaning. In particular, to see the effect of the variation of frequency on the accuracy of the method developed here, for example, two frequencies could considered for fixed Δh and d, say 0.9 GHz and 1.8 GHz. For both frequencies, the relative accuracy of the method is the same. However, this could reduce the number of edges to be eliminated for each frequency.

Table 6 Comparison of UTD based models for accuracy, 9 diffractions

TRW	μ (dB) (S-UTD-CH)	σ (dB) (S-UTD-CH)	μ (dB) (UTD)	σ (dB) (UTD)	Edge (#)
0.2	0.01	0.01	4.97	2.22	0.2
0.3	0.01	0.02	4.31	3	0.3
0.5	0.04	0.05	3.21	3.14	0.8
1.1	0.09	0.12	3.92	2.5	2
1.3	0.08	0.09	3.42	3.73	1.7
2.2	0.09	0.09	1.35	1.03	3.1
2.5	0.11	0.18	1.47	1.35	2.9
4.3	0.09	0.08	1	0.79	3.9
4.9	0.13	0.18	1.29	1.31	2.2
5	0.09	0.09	1.29	0.86	4.3
8.6	0.14	0.3	1.48	1.24	3.9
9.7	0.09	0.09	1.16	1.47	3.5
10.1	0.14	0.12	0.91	1.35	4.6

Table 7 Comparison of UTD based models for computation time, 9 diffractions

TRW	Time (s) (S-UTD-CH)	Time (s) (S-UTD)	Time(s) (UTD)	Edge (#)
0.2	937	1113	5	0.2
0.3	963	1166	5.6	0.3
0.5	619	1121	5.3	0.8
1.1	179	1134	5.5	2
1.3	209	1192	6	1.7
2.2	109	1085	5.2	3.1
2.5	46.1	1093	5.1	2.9
4.3	3.4	1111	5.4	3.9
4.9	95	1043	5	2.2
5	2.4	1092	5.5	4.3
8.6	32	1006	4.5	3.9
9.7	23.2	1076	5	3.5
10.1	3.9	1040	4.9	4.6

5. 1. 2 Knife-edges distributed with unequal spacing

All simulations are conducted for a canonical multiple edge transition zone diffraction geometry including 13 knife edges. These simulations are performed in C++ environment. Tables 8 and 9 give the simulation results with respect to accuracy and computation time. The first and second rows represent simulations for the frequency 2.1 GHz and 1.8 GHz and the difference between the building heights is 6 m. The third and fourth rows represent simulations for the frequency 2.1 GHz and 1.8 GHz and the difference between the building heights is 3 m. There were 10 runs for each case.

In Table 8, leftmost column gives the TRW values. Mean error and standard deviation of excess loss for UTD is given in the next two columns. Mean error and standard deviation of excess loss for S-UTD-CH is given in fourth and fifth columns. The rightmost column gives the eliminated knife edge number in model S-UTD-CH. There is at most only 0.1 dB mean error even if 7 knife edges are eliminated. As the frequency increase, eliminated edge number and TRW decreases due to fact that Fresnel zone radius is reduced. Also it can be seen from the table, for the smaller TRW values, UTD

gives relatively larger mean error because of that knife edges being in the transition region of the previous ones.

Table 8 Comparison of UTD based models for accuracy, 13 diffractions

TRW	μ (dB) (UTD)	σ (dB) (UTD)	μ (dB) (S-UTD-CH)	Σ (dB) (S-UTD-CH)	Edge (#)
10,08	-0,55	0,56	-0,02	0,12	8,0
8,64	-1,47	1,83	-0,10	0,27	7,1
2,52	-6,30	4,11	0,01	0,10	5,1
2,16	-4,84	3,92	-0,08	0,11	4,5

In Table 9, leftmost column gives the TRW values. Mean of computation time for UTD is given in the next column. Mean of computation time for S-UTD-CH is given in third column. The rightmost column gives the eliminated knife edge number in model S-UTD-CH. As can be seen from the table, computation time for S-UTD-CH is relatively smaller the S-UTD (1 sec for S-UTD-CH to 16615 sec for S-UTD), with only 0.02 dB mean error. For the larger TRW values, S-UTD-CH is the fastest one among the three models.

Table 9 Comparison of UTD based models for computation time, 13 diffractions

TRW	Time (s) (UTD)	Time (s) (S-UTD)	Time (s) (S-UTD-CH)	Edge (#)
10,08	16	16615	1	8,0
8,64	19	22862	5	7,1
2,52	35	45401	110	5,1
2,16	34	42869	191	4,5

5. 2 Comparison of the UTD Based Models with PO

Another class of models to solve multiple edge diffraction problems is based on

numerical evaluation of physical optics (PO) integrals or so-called PO solutions [11]. Since these models involve numerical computation of PO integrals at each point in the field domain, they are considered to have ultimate accuracy [11]. However, these models have extremely large computation times compared with UTD based models. In this section, accuracies of improved UTD models are compared with a PO model that has been reported in [11].

In this sense, this would be the first time that the accuracy of ray theoretic models, i.e. S-UTD and S-UTD-CH, is statistically compared with a well-known PO model for multiple edge diffraction problems. In simulations, structural parameters of screens for the PO model proposed in [11] were chosen appropriately to simulate absorbing knife edges.

The canonical multiple edge geometry previously used with the following parameters:
The transmitting antenna height (h_T): 5 and 10m
Heights of edges (h): uniformly distributed over [10-Δh, 10+Δh] with Δh=4m
Distance between the edges (d): 50m
Operating frequency (f): 1.8GHz
Receiver height is the height of the last randomly distributed edge.

Firstly, randomly distributed edge heights for 10 equally-spaced edges are generated. Then, the field strength is calculated at the tip of the last edge using the three models for given height distributions. There was a total of 25 height distributions generated in simulations. The PO model is taken as the reference model since it is a fully numerical algorithm and highest accuracy compared with the ray models (S-UTD-CH and S-UTD). Then, the mean error (μ) and standard deviation (σ) for excess loss predicted by ray theoretic models, i.e. S-UTD-CH and S-UTD, are calculated accordingly. Table 10 presents the results of the simulations for two transmitting antenna heights. Here, since the motivation was to investigate the accuracy of S-UTD compared with PO for multiple edge transition zone diffraction, only lower transmitting antenna heights (h_T =5, 10m) are considered (transition zone diffraction situation). For elevated transmitting antenna heights, UTD is satisfactory for most cases and the field predicted is less dependent on

transition zone diffraction effects. Because direct rays or single diffracted rays are considered to be dominant in this case, and their contributions to the received field strength are relatively larger than higher order rays.

Table 10 Comparison of ray theoretic models with the PO model

h_T(m)	μ (dB) (S-UTD-CH)	σ(dB) (S-UTD-CH)	μ (dB) (S-UTD)	σ(dB) (S-UTD)
5	0.42	7.51	0.58	7.43
10	0.55	7.29	0.60	7.28

As shown in Table 10, S-UTD exhibits a mean error of less than 0.6 dB after 9 diffractions. Simulations were carried out up to 9 diffractions since S-UTD has an increasing error after 9 diffractions for equally-spaced edge geometry. This error inherent in S-UTD was one of the motivations in developing S-UTD-CH algorithm in [7]. As it is well-known, PO model requires very large computation times since it is based on computation of field at each point over the knife edges. Therefore, S-UTD and PO were not compared for computation time.

A rather fast and a similar algorithm based on selection of dominant edges (isolated diffracting edges-IDE) contributing much to the field strength has been proposed and compared with the PO model in [30]. However, the accuracy of the model was reported to be unsatisfactory, especially, for lower transmitting antenna heights where transition zone diffraction is the dominant mechanism. It was the transition zone diffraction effects that cause this error.

5. 3 Comparison of S-UTD-CH with PO

The canonical multiple edge geometry is used with the same parameters this time for elevated transmitting antennas (h_T): 15 and 20m. Again randomly distributed edge heights for 15 equally-spaced edges are generated. Then, the field strength is calculated at the top of the last edge using the two models (S-UTD-CH and PO) for the height

distribution. There was a total of 20 height distributions generated in simulations. Then, the mean error (μ) and standard deviation (σ) for excess loss predicted by ray theoretic models, i.e. S-UTD-CH, are calculated accordingly. Simulations are made in C/C++ environment. Table 11 presents the results of the simulations for elevated two transmitting antenna heights.

In Table 11, leftmost column shows the transmitter height. Next three column shows the average computation time. Next two columns shows mean error and standard deviation for excess loss predicted by S-UTD-CH (as PO being the reference solution). S-UTD-CH exhibits a mean error of less than 1.33 dB after 14 diffractions. On the other hand, S-UTD-CH is faster than the PO model.

Table 11 Comparison of S-UTD-CH with the PO for accuracy and computation time (14 diffractions)

h_T(m)	μ (s) (S-UTD-CH)	μ (s) (PO)	μ (dB) (PO)	σ(dB) (PO)
15	789	802	1.33	7.36
20	4	802	-1.27	7.53

CHAPTER 6

3D MODELS

In this chapter, review of algorithms for 3D ray tracing in urban environment, and design considerations for the development of 3D ray tracing package are discussed. As in 2D applications, there are two types of prediction algorithm for 3D applications for indoor, urban, suburban and rural environments. One is ray theoretical models based on 3D ray tracing; the other is numerical models based on computation of Fresnel-Kirchhoff integrals.

6. 1. 3D Ray Theoretical Models

A 3D ray tracing technique is proposed in [31]. The model applies Geometrical Optics (GO) and UTD in order to calculate the relative path loss of the electromagnetic waves originated from the base station (BS) at the mobile station (MS). In order to determine the geometry of the rays, a hybrid imaging technique has been developed according to which 2-D image generations in vertical and horizontal planes are combined to produce 3-D paths [31].

Another ray tracing algorithm is presented in [32]. For the calculation of each ray contribution to total field, a combination of geometrical optics (GO) and uniform geometrical theory of diffraction (GTD) is applied. The reflecting surfaces are assumed to be planar and smooth, characterized by their special conductivity and relative electrical permittivity. The location of every reflection or diffraction point is carried out using a ray-tracing method based on Snell's law of reflection and Keller's law of

diffraction [32]. Top view of the site and all the rays contributing to total field is showed in Fig. 25.

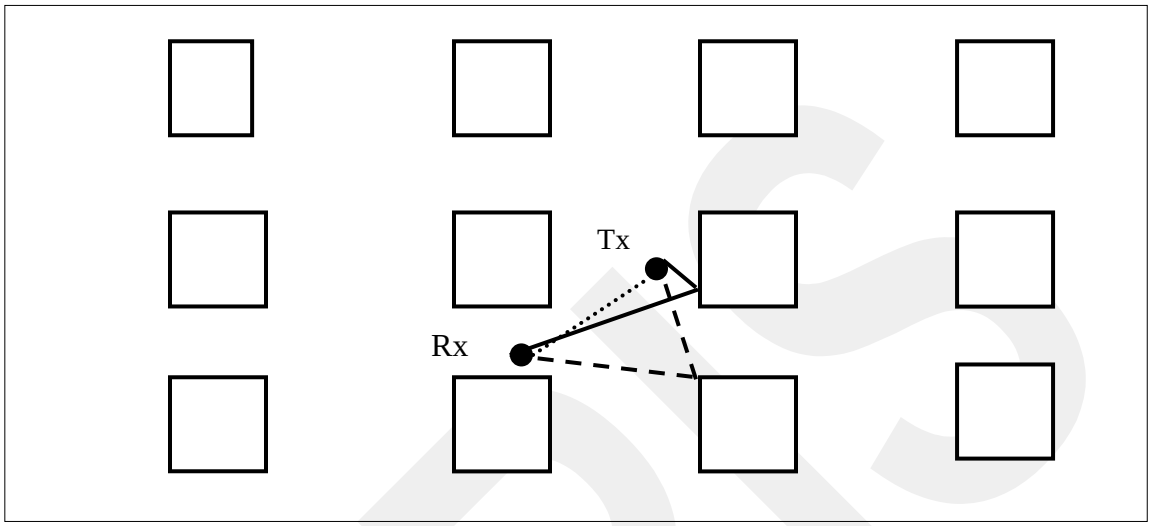

Fig. 25 Top view of the site

As can be seen from the Fig. 25, a specific location of the base station (Tx), mobile station (Rx) and some typical ray paths are illustrated. 11 ray categories have been considered as following;

- Direct
- Reflected
- Corner-diffracted
- Rooftop-diffracted
- Doubly reflected
- Doubly corner-diffracted
- Doubly rooftop-diffracted
- Reflected/corner-diffracted
- Corner-diffracted/reflected
- Rooftop-diffracted/reflected
- Rooftop-diffracted/corner-diffracted.

These rays can be determined via ray tracing algorithm as shown in Fig. 26. The locations of the transmitter, the receiver and the site including the height and width is entered, then ray tracing algorithm runs and all the rays contributing total field determined.

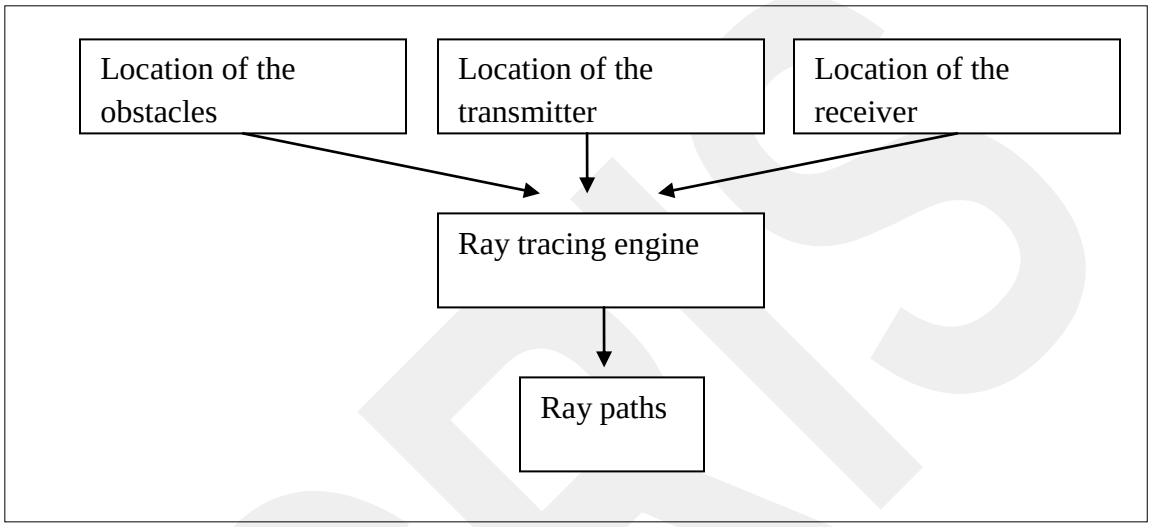

Fig. 26 Block diagram of the Ray tracing algorithm

After determining the rays contributing to total field, via this rays total field can be calculated as shown in Fig. 27. Ray paths are taken from ray tracing engine and frequency is entered then path loss algorithm calculates the total field.

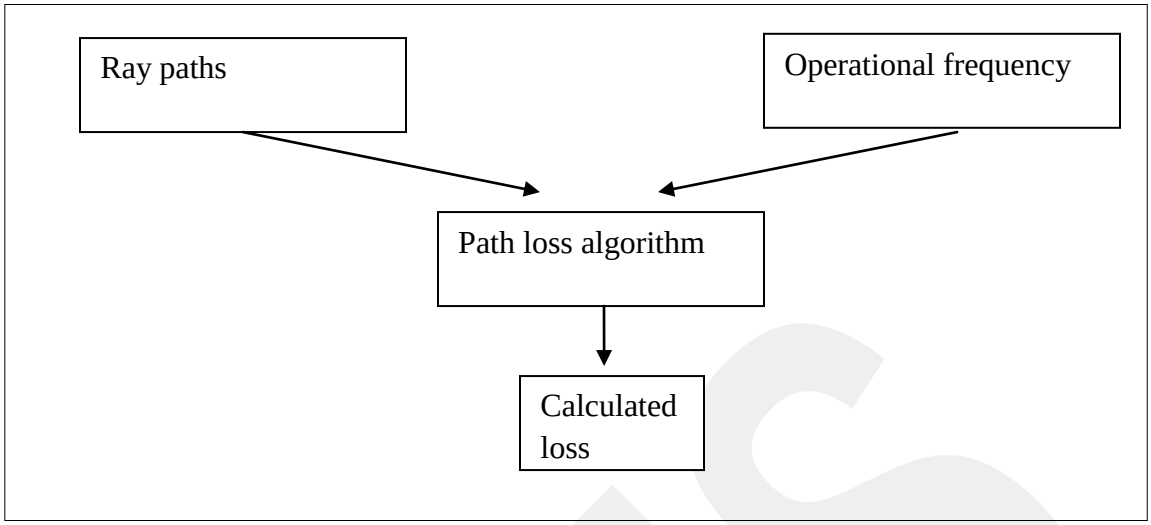

Fig. 27 Block diagram of the Path Loss algorithm

There are three types of ray fields, LOS, reflected and diffracted. These fields can be calculated via the equation is given

$$E_{LOS} = E_0 \frac{e^{-jkd}}{d} \tag{22-a}$$

$$E_R = E_0 R \frac{e^{-jk(s+s')}}{s+s'} \tag{22-b}$$

$$E_D = E_0 D \sqrt{\frac{s}{s(s+s')}} \frac{e^{-jk(s+s')}}{s'} \tag{22-c}$$

where, *d* is propagation path length,

Only using roof-top diffracted or corner diffracted field is not enough for predicting the total field. All of the cases mentioned above have to be considered.

Another model for ray tracing is presented in [33]. In that model, firstly, computation efficient of the (2D) ray tracing model improved by reorganizing the objects in an indoor environment into irregular cells. Secondly, by making use of the two-dimensional ray-tracing results, a new three-dimensional (3D) propagation prediction model is developed. This model saves 99% of the computation time of a traditional three-dimensional numerical model. This model is more accurate than two-dimensional

models, and more efficient in computing the path loss to any point in obstacle than traditional three-dimensional models. In this model, also reflection, refraction and diffraction are considered as shown in Fig. 28.

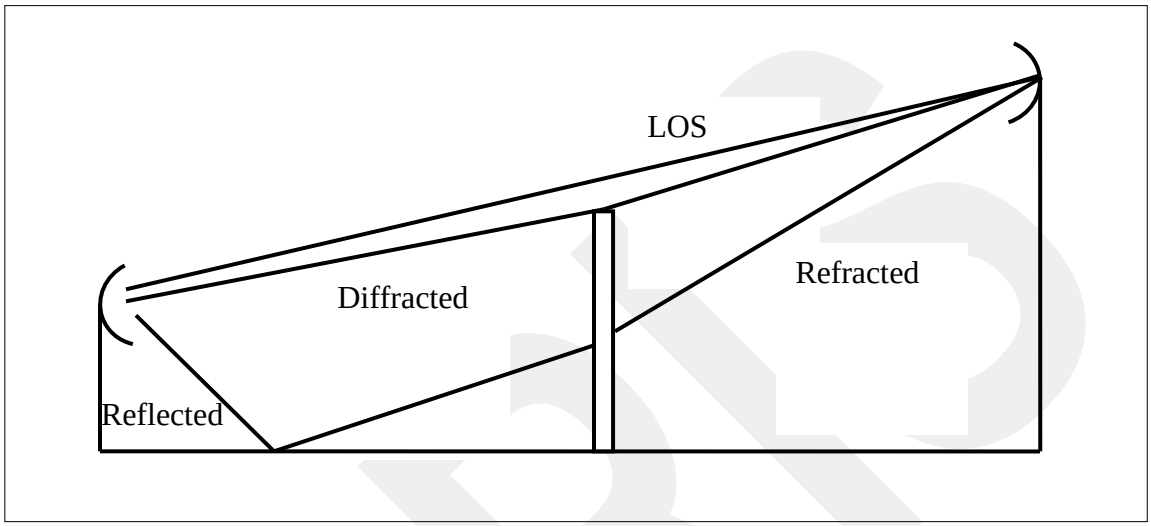

Fig. 28 Rays for 3D

6. 2. 3D Numerical Solutions

Most deterministic models for the prediction of electromagnetic wave propagation in urban, suburban and rural environments are based either on ray-tracing as mentioned above or on integral models. One difficulty of ray-tracing models, when they are applied to a 3D scenario, comes from the existence of Keller's cone [34]. Integral models, on the other hand, have a very high computational time when many obstacles are present in the geometry. Fresnel-Kirchhoff integral is used to compute path loss from buildings in 3D urban and suburban environment. In this case both diffraction and reflection are considered. This numerical model proposed in [34, 35] for 3D field prediction is in good agreements with the measurements. There are only a few dB errors with measurements.

CHAPTER 7

CONCLUSIONS

Multiple-diffraction has been considered in many radio propagation models for radio network planning in radio communications and broadcasting systems. To make more reliable and time-efficient systems, many radio propagation models have been proposed for urban, suburban, rural and indoor applications. These models can be classified in two groups like ray theoretical and numerical models. Ray theoretical models are based on ray tracing like UTD, whereas numerical models based on solving Fresnel and Kirchhoff-Huygen like integrals like PO. Even though ray theoretical models are time efficient, their accuracy of field prediction is not in a good agreement with real measurements. There is a tradeoff between the computation time and accuracy and computation complexity and accuracy of prediction. Models having higher accuracy with large computation time seem to be infeasible in many cases including area coverage predictions in radio propagation. In this thesis, UTD based models are explained and compared with each other. Firstly, UTD model is described. Even if one obstacle is in the transition region of the previous, UTD fails to predict the field strength correctly. It has been shown in simulations that although it is the fastest model for prediction of field, there are approximately 5 dB errors with real measurements. Then, S-UTD model proposed in [5] is explained. In addition to UTD, in this model slope terms are added and most of the discontinuity in the transition region is removed. This model gives approximately 1 dB error in prediction of field as seen in simulations. This error resulted from the calculation of the distance parameters. To calculate the distance parameters, amplitude, slope and phase continuity equations have to be solved at the shadow boundary points as in Appendix B. In the case [5], phase continuity is not taken account. Next, S-UTD model proposed with meeting the phase continuity in [7, 8] is explained.

As is shown parabolic tests, S-UTD contribution to total field strength is most in the transition region. As it has been showed in simulations, this model is in good agreement with the real measurements (PO). It is reported in [10] that S-UTD model loses the accuracy as the number of obstacles in the environment is greater than 9. Furthermore, S-UTD model requires higher computation time for the geometry including more obstacles. S-UTD model has relatively higher computation time than UTD model. For 13 diffractions UTD model requires 16 sec, whereas S-UTD model 16615 sec.

In this thesis, effects of conductivity, relative permittivity constant and interior wedge angle of the wedges are analyzed. As the conductivity, relative permittivity constant and interior angle of wedge type obstacles are increased, relative path loss at the receiver is decreased.

Finally, we have proposed a new model for multiple diffraction for indoor, urban, suburban and rural areas, is called S-UTD-CH. S-UTD-CH model is based on convex hull method and S-UTD model. S-UTD-CH that uses a selection algorithm of diffracting obstacles based on Fresnel zone concept would be used for transition zone diffraction. S-UTD-CH provides not only very low computation time but also very accurate results for multiple diffractions (greater than 9 knife edge or wedges) due to that after 9 diffractions S-UTD loses accuracy.

As is shown in simulations, for smaller TRW values, contribution of S-UTD and S-UTD-CH approximately 4.9 dB cannot be ignored. For multiple transition diffraction, S-UTD-CH has larger computation time with higher accuracy while UTD has small computation time with lower accuracy.

Moreover, UTD based models are compared after 13 diffractions for computation time and accuracy. There is at most 0.1 dB between the S-UTD and S-UTD-CH model. However there is huge difference between the computation times (22862 to 5 sec). For some TRW values, S-UTD-CH model is faster than the UTD model (19 to 5 sec).

On the other hand, S-UTD and S-UTD-CH have been compared with the PO [11] for the first time for accuracy in this thesis. It has been shown that S-UTD-CH and S-UTD exhibits very small error after 9 diffractions (0.58 and 0.42 dB).

Furthermore, S-UTD-CH has been compared with PO for accuracy and computation time. It has been shown that S-UTD-CH shows very small error (1.33 dB) after 14 diffractions with less computation time.

As can be seen all simulation, S-UTD-CH is faster than S-UTD, and gives more accurate results than UTD model. Also S-UTD-CH gives more accurate results after 9 diffractions than S-UTD. Moreover, S-UTD-CH gives result are in good agreement with a numerical model PO. It can be say; S-UTD-CH is optimum model for its computation time and accuracy of field prediction.

As can be seen in chapter 6, this ray theoretical based on ray tracing and numerical models based on computation of the Fresnel-Kirchhoff integral can be applied to 3D scenarios. As in 2D geometries, ray theoretical models faster than the numerical models. Then future work will be about modeling of S-UTD-CH for 3D geometries.

REFERENCES

[1] Andersen, J. B., "Transition zone diffraction by multiple edges", IEEE Proceedings - Microwave Antennas and Propagation, Vol. 141, No 5, pp. 1093–1097, October 1994.

[2] Kouyoumjian, R. G., Pathak, P. H., "A uniform geometrical theory of diffraction for an edge in a perfectly conducting surface", Proceedings of the IEEE, Vol. 62, pp. 1448–1461, 1974.

[3] Torabi, E., Ghorbani A., Amindavar, H. R., "Modification of the UTD Model for Cellular Mobile Communication in an Urban Environment", Electromagnetics, Vol. 27, No. 5, pp. 263-285, 2008.

[4] Rodríguez, J. V., Molina-García-Pardo, J. M., Juan-Llácer, L., "An Improved Solution Expressed in Terms of UTD Coefficients for the Multiple-Building Diffraction of Plane Waves", IEEE Antennas and Wireless Communications, Vol. 4, pp. 16-19. 2005.

[5] Andersen, J. B. "UTD multiple-edge transition zone diffraction", IEEE Transactions on Antennas and Propagation, Vol. 45, pp. 1093–1097, 1997.

[6] Holm, P. D., "UTD-Diffraction Coefficients for Higher Order Wedge Diffracted Fields", IEEE Transactions on Antennas and Propagation, Vol. 4, No. 6, pp. 879-888, 1996.

[7] Rizk, K., Valenzuela, R., Chizhik, D., Gardiol, F., "Application of the slope diffraction method for urban microwave propagation prediction", IEEE Vehicular Technology Conference, Vol. 2, pp. 1150–1155, 1998.

[8] Tzaras, C., Saunders, S. R., "An improved heuristic UTD solution for multiple-edge transition zone diffraction", IEEE Transactions on Antennas and Propagation, Vol. 49, No. 12, pp. 1678–1682, 2001.

[9] Vogler, L. “An attenuation function for multiple knife-edge diffraction”, Radio Science, Vol. 17, pp. 1541–1546, 1982.

[10] Kara, A., Yazgan, E., Bertoni, H. L., “Limit and application range of slope diffraction for wireless communication”, IEEE Transactions on Antennas and Propagation, Vol. 51, No. 9, pp. 2512-2514, 2003.

[11] Chung, H. K., Bertoni, H. L., “Range-dependent path-loss model in residential areas for the VHF and UHF bands”, IEEE Transaction on Antennas and Propagation, Vol. 50, No. 1, pp. 1–11, 2002

[12] Tzaras, C., Saunders, S. R., “Comparison of Multiple-Diffraction Models for Digital Broadcasting Coverage Prediction”, IEEE Transactions on Broadcasting, Vol. 46, No. 3, pp. 221-226, 2000

[13] Tabakcioglu, M. B., Kara, A., “On the improvements in the multiple edge transition zone diffraction”, EuCAP’07, pp. 1-5, November, 2007

[14] Tabakcioglu, M. B., Kara, A., “Comparison of Various UTD and PO Solutions for Multiple-Edge Transition Zone Diffraction”, APS/URSI’08, July, 2008

[15] Tabakcioglu, M. B., Kara, A., “Discussions of Various UTD and PO Solutions for Multiple-Edge Diffractions in Urban Radio Propagation Modeling”, EWS’08, 11, pp. 1-6 October, 2008

[16] Tabakcioglu, M. B., Kara, A., “Improvements on Slope Diffraction for Multiple Wedges”, (Submitted).

[17] Tabakcioglu, M. B., Kara, A., “An Improved Slope UTD Method for Multiple Building Diffractions”, Electromagnetics,(To be published).

[18] Tabakcioglu, M. B., Kara, A., “A new Slope Diffraction Model for Coverage in Broadcasting Systems”, SIU’2009, Antalya, submitted.

[19] Karousos, A., Tzaras, C., “Multi Time-Domain Diffraction for UWB Signals”, IEEE Transactions on Antennas and Propagation, Vol. 56, No. 5, pp. 1420-1427, 2008.

[20] Koutitas, G., Tzaras, C., "A Slope UTD Solution for a Cascade of Multishaped Canonical objects", IEEE Transactions on Antennas and Propagation, Vol. 54, No. 10, pp. 2969-2976, 2006.

[21] Tajvidy, A., Ghorbani, A., "A New Uniform Theory-of-Diffraction-Based Model for the Multiple Building Diffraction of Spherical Waves in Microcell Environments", Electromagnetics, Vol. 28, No. 5, pp. 375-387, 2007.

[22] Sklar, B., "Digital Communications Fundamentals and Applications", New Jersey, Prentice Hall PTR, 2001.

[23] Haykin, S., Moher, M., "Modern Wireless Communications", New Jersey, Pearson Prentice Hall, 2005.

[24] Bertoni, H. L., "Radio propagation for modern wireless systems", New Jersey, Prentice Hall, 2000.

[25] Holm, P. D., "Calculation of Higher Order Diffracted Fields for Multiple-Edge Transition Zone Diffraction", IEEE Transactions Antennas and Propagation, Vol. 52, No. 5, pp. 1350-1355, 2004.

[26] Holm, P. D., "A New Heuristic UTD Diffraction Coefficient for Nonperfectly ConductingWedges", IEEE Transactions on Antennas and Propagation, Vol. 48, No. 8, pp. 1211-1219, 2000.

[27] McNamara, D. A., Pistorious, C. V., Malherbe, J. A. G., "Introduction to the Uniform Geometrical Theory of Diffraction", Boston, MA: Artech House, 1990.

[28] Luebbers, R. J., "A Heuristic UTD Slope Diffraction Coefficient for Rough Lossy Wedges", IEEE Transaction on Antennas and Propagation, Vol. 37, No. 2, pp. 206–211, 1989.

[29] Luebbers, R. J., "A General, Uniform Double Wedge Diffraction Coefficient", IEEE Transaction on Antennas and Propagation, Vol. 39, No. 1, pp. 8–14, 1991.

[30] Chung, H. K., Bertoni, H. L., "Application of isolated diffraction edge method for urban microwave path loss prediction", IEEE Vehicular Technology Conference, pp. 205–209, 2003.

[31] Athanasiadou, G. E. and Nix, A. R., "A Novel 3-D Indoor Ray-Tracing Propagation Model: The Path Generator and Evaluation of Narrow-Band and Wide-Band Predictions", IEEE Transactions on Vehicular Technology, Vol. 49, No. 4, pp. 1152–1168, July 2000.

[32] Kanatas, A. G., Kountouris, I. D., Kostaras, G. B, Constantinou, P., "A UTD Propagation Model in Urban Microcellular Environments," IEEE Transactions on Vehicular Technology, Vol. 46, No. 1, pp. 185–193, February 1997.

[33] Ji, Z., Li, B. H., Wang, H. X., Chen, H. Y., Sarkar, T. K., "Efficient Ray-Tracing Methods for Propagation Prediction for Indoor Wireless Communications ", IEEE Antennas and Propagation Magazine, Vol. 43, No. 2, April 2001

[34] Xu, Y., Tan, Q., Erricolo, D., Uslenghi, P. L. E. "3D Propagation in Urban Environments Using Fresnel-Kirchhoff Integrals", IEEE Topical Conference on Wireless Communication Technology, 2003

[35] Xu, Y., Tan, Q., Erricolo, D., Uslenghi, P. L. E. , "Experimental Verification of A 3-D Propagation Model Based on Fresnel-Kirchhoff Integral," IEEE Antennas and Propagation Society International Symposium**,** Vol. 4, pp. 3653-3656, June 2004

Appendix A
TRANSITION FUNCTION

Transition function is a special function is used both knife edge and wedge diffraction [27] is given by,

$$F(x) = 2j\sqrt{x}e^{jx}\int_{\sqrt{x}}^{\infty} e^{-ju^2}du \quad \text{(A.1)}$$

where,

$x = 2kLcos^2(\alpha/2)$ for the knife edge case,

$x = 2kLn^2\, sin^2(\psi(i))$ for the wedge case.

$$\psi(1)=\frac{\pi+\varphi-\varphi'}{2n},\ \psi(2)=\frac{\pi-\varphi+\varphi'}{2n},\quad \psi(3)=\frac{\pi-\varphi-\varphi'}{2n},\ \psi(4)=\frac{\pi+\varphi+\varphi'}{2n} \quad \text{(A.2)}$$

k is wave number, α is the angle between the diffracted and incoming wave. *L* is the distance parameter for amplitude diffraction coefficient as calculated in Appendix B. *n* in (A.2) is a number is related with the wedge angle is given by

$$n = 2 - \beta/\pi \quad \text{(A.3)}$$

The transition function can be calculated the following script we developed,

```
function fres=fresnel(x)

  if x>10
     fres=1+eps;
  elseif x<0.00000001
      fres=sqrt(pi*x)*exp(j*(pi/4+x));
  else

     xn=sqrt(x);x0=0;n=100;
     h=(xn-x0)/n;
     sums=0.5*h*(sin(xn^2)+sin(x0^2));
     sumc=0.5*h*(cos(xn^2)+cos(x0^2));
     t=h;
```

```
    for i=1:n-1,
        sums=sums+h*sin(t^2);
        sumc=sumc+h*cos(t^2);
        t=t+h;
    end

    ex=sumc-j*sums;
    c1=sqrt(pi*x)*exp(j*(pi/4+x));
    c2=2*j*sqrt(x)*exp(j*x);
    fres=c1-c2*ex;
end
```

as can be seen from the script, some properties of the transition functions are given

- For small *x* values (close to shadow boundaries)

$$F(x) = 0 \tag{A.4}$$

- For large *x* values (far from shadow boundaries)

$$F(x) \cong 1 \tag{A.5}$$

- Otherwise,

$$F(x) = 2j\sqrt{x}e^{jx}\int_{\sqrt{x}}^{\infty} e^{-ju^2}du. \tag{A.6}$$

Derivative of the transition function is given by,

$$\frac{\partial F_{x_i}}{\partial \varphi'} = \frac{\partial x_i}{\partial \varphi'}\left(\frac{F(x_i)}{2x_i} + j(F(x_i) - 1)\right) \tag{A.7}$$

where, $\frac{\partial x_i}{\partial \varphi'} = \pm kLn \sin 2\psi_i$ for $i = 1$ and 3 the minus sign shall be taken into account, whereas for $i = 2$ and 4 the plus one.

Appendix B

DISTANCE PARAMETERS

There are two cases for the calculation of the distance parameters L and L_s for the amplitude and slope diffraction coefficients. We have derived formulas to calculate the distance parameters for these two cases. The first case is that all the buildings are in unequal heights and spacing. The other case is for equal heights and spacing.

- **Unequal heights and spacing case**

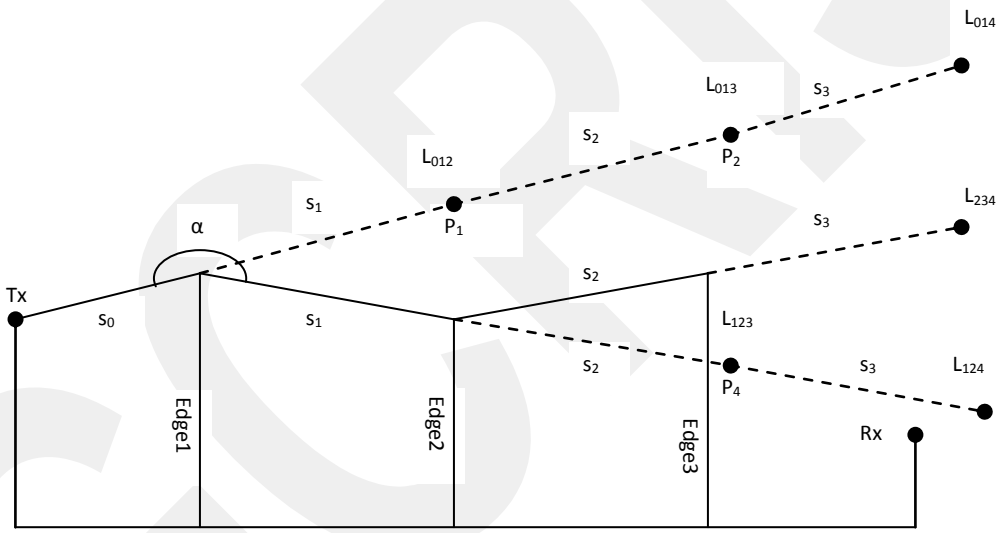

Fig.1. Ray geometry of multiple knife edge diffraction

L and L_s parameters are distance parameters for amplitude and slope diffraction coefficient and have to be calculated via taking into account amplitude, slope and phase continuities [7, 8]. Distance parameters have to be calculated numerically both for knife-edge and wedge cases. Continuity equations vary for each ray independently. Firstly, shadow boundary points like P_1, P_3 and P_4 as shown in Fig. 1 are determined as following. The ray originated from the transmitter is extended in the same direction at a distance from the diffracting edge to the observation point. The final position of the ray

is the shadow boundary point. Secondly, electric field is calculated at this shadow boundary points. Finally, continuity equations are solved and the distance parameters are calculated. Amplitude continuity equation is that half of the direct field from the transmitter is equal to the diffracted field at the shadow boundary points. In the same way, slope continuity equation is that half of the derivative of the direct field from the transmitter is equal to the derivative of the diffracted field at the shadow boundary points. For instance, L_{012} parameter for amplitude diffraction coefficient can be calculated as following. Firstly, shadow boundary point P_1 is determined. Then the direct field from the transmitter, E_{02} at the shadow boundary point P_1 is calculated as given

$$E_{02} = \frac{E_0}{s_0+s_1} e^{-jk(s_0+s_1)} \tag{B.1}$$

Next, diffracted field from the first edge is calculated at point P_1 is given

$$E_{012} = E_{01} D(\alpha_{012}, L_{012}) A_{012} e^{-jk(s_1)} \tag{B.2}$$

The continuity equation for amplitude diffraction coefficient is given

$$\frac{1}{2} E_{02} = E_{012} \text{ at point } P_1. \tag{B.3}$$

In the case the diffracting angle $\alpha = \pi$ amplitude diffraction coefficient reduced to

$$D(\alpha_{012}, L_{012}) = \frac{1}{2}\sqrt{L_{012}} \tag{B.4}$$

Finally, continuity equation in (B.3) is solved via inserting (B.4) into (B.2) and distance parameters for amplitude diffraction coefficient can be calculated.

As another example, L_{0123} parameter for amplitude diffraction coefficient can be calculated as following. Firstly, shadow boundary point P_4 is determined. Then the direct field from the transmitter E_{013} at the shadow boundary point *P4* is calculated as given

$$E_{013} = E_{01} D(\alpha_{013}, L_{013}) A_{013} e^{-jk(s_1+s_2)} \tag{B.5}$$

Next, diffracted field from the first and second edge is calculated at point P_4 is calculated as given

$$E_{0123} = E_{012} D(\alpha_{123}, L_{0123}) A_{0123} e^{-jk(s_2)} \tag{B.6}$$

The continuity equation for amplitude diffraction coefficient is given

$$\frac{1}{2} E_{013} = E_{0123} \text{ at point } P_4 \tag{B.7}$$

In the case the diffracting angle $\alpha = \pi$ amplitude diffraction coefficient reduced to

$$D(\alpha_{123}, L_{0123}) = \frac{1}{2}\sqrt{L_{0123}} \tag{B.8}$$

Finally, continuity equation in (B.7) is solved via inserting (B.8) into (B.6) and distance parameters for amplitude diffraction coefficient can be calculated.

As another example, $L_{s_{0123}}$ parameter for slope diffraction coefficient can be calculated as following. Firstly, shadow boundary point P_4 is determined as previously. Then the derivative of the direct field from the transmitter E_{013} at the shadow boundary point P_4 is calculated as given

$$\frac{\partial E_{013}}{\partial \alpha} = E_{01} \frac{\partial D(\alpha_{013}, L_{013})}{\partial \alpha} A_{013} e^{-jk(s_1+s_2)} \tag{B.9}$$

Next, the derivative of the diffracted field from the first edge is calculated at point P_4 is calculated as given

$$\frac{\partial E_{0123}}{\partial \alpha} = E_{01} \frac{\partial D(\alpha_{012}, L_{012})}{\partial \alpha} A_{012} e^{-jk(s_1)} \frac{\partial d_s}{\partial \alpha} A_{0123} e^{-jk(s_2)} \tag{B.10}$$

The continuity equation for slope diffraction coefficient is given

$$\frac{1}{2} \frac{\partial E_{013}}{\partial \alpha} = \frac{\partial E_{0123}}{\partial \alpha} \text{ at point } P_4 \tag{B.11}$$

In the case the diffracting angle $\alpha = \pi$ slope diffraction coefficient reduced to

$$\frac{\partial d_s}{\partial \alpha} = \frac{1}{2} L_{s_{0123}}{}^{3/2} \tag{B.12}$$

Finally, continuity equation in (B.11) is solved via inserting (B.12) into (B.10) and distance parameters for amplitude diffraction coefficient can be calculated.

In the same way distance parameters can be calculated for the wedge case as in Fig. 2.

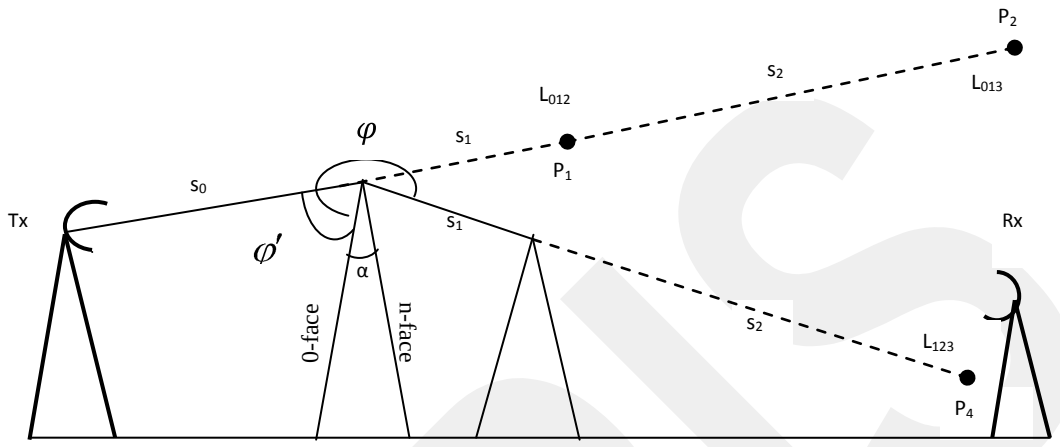

Fig.2. Ray geometry of multiple wedge diffraction

Instead of the solving the continuity equations, distance parameters for the amplitude and slope diffraction coefficients for knife edge and wedge case can be calculated via using the formulas are provided in [13-18] is given

$$L_{0jk} = \frac{r_{0j} r_{jk}}{r_{0k}} \tag{B.13-a}$$

$$L_{0ijk} = \left(\frac{D(\alpha_{0ik}, L_{0ik}) A_{0ik}}{D(\alpha_{0ij}, L_{0ij}) A_{0ij} A_{0ijk}} \right)^2 \tag{B.13-b}$$

$$L_{s_{0ijk}} = \left(\frac{ds(\alpha_{0ik}, L_{0ik}) A_{0ik}}{ds(\alpha_{0ij}, L_{0ij}) A_{0ij} A_{0ijk}} \frac{r_{ij}}{r_{ik}} r_{jk} \right)^{2/3} \tag{B.13-c}$$

$$L_{s,\mathrm{h}_{0ij}} = \frac{r_{0j} r_{jk}}{r_{0k}} \tag{B.14-a}$$

$$L_{s,h_{0ijk}} = \left(\frac{D_{s,h}(L_{s,h_{0ik}}) A_{0ik}}{D_{s,h}(L_{s,h_{0ij}}) A_{0ij} A_{0ijk}} \right)^2 \tag{B.14-b}$$

$$L_{s_{s,h_{0ijk}}} = \left(\frac{d_{s_{s,h}}(L_{s,h_{0ik}}) A_{0ik} r_{ij} r_{jk}}{d_{s_{s,h}}(L_{s,h_{0ij}}) A_{0ij} A_{0ijk} r_{ik}} \right)^{2/3} \tag{B.14-c}$$

where i, j and k are the indices for the source, diffracting and shadow boundary points. r_{ij} is the distance between the source and diffracting points. D and ds are amplitude and slope diffraction coefficient for the knife edge. $D_{s,h}$ and $d_{s_{s,h}}$ are amplitude and slope diffraction coefficient for wedge case with soft or hard polarization, the respectively. As can be seen from the equations above, distance parameters are calculated recursively.

- **Equal heights and spacing case**

The equal heights and spacing case is the simplest case for knife edge and wedge case and the distance parameters can be calculated analytically as follow.

$$L_{0ijk} = \frac{\sum_{i=0}^{j-1} s_i \sum_{i=j}^{k-1} s_i}{\sum_{i=0}^{k-1} s_i} \tag{B.15}$$

$$L_{s_{0ijk}} = \left(\frac{\sum_{m=0}^{k-1} s_m}{\sum_{m=0}^{k-1} s_m}\right)^{2/3} \left(\frac{\sum_{m=i}^{j-1} s_m}{\sum_{m=i}^{j-1} s_m}\right)^{1/3} \sum_{m=j}^{k-1} s_m \tag{B.16}$$

Appendix C

DERIVATIVE OF THE SLOPE DIFFRACTION COEFFICIENT

To calculate the slope terms of the S-UTD model, after 2 diffractions derivative of the slope diffraction coefficient is required. Derivative of the slope diffraction coefficient with respect to φ' for soft and hard polarization are given by,

$$\frac{\partial ds_s}{\partial n} = \frac{1}{s}\left[\begin{array}{c}\frac{\partial^2 R_{0s}}{\partial \varphi'^2} R_{ns} D_1 + 2\frac{\partial R_{0s}}{\partial \varphi'} R_{ns}\frac{\partial D_1}{\partial \varphi'} + R_{0s} R_{ns}\frac{\partial^2 D_1}{\partial \varphi'^2} + \frac{\partial^2 D_2}{\partial \varphi'^2} + \\ \frac{\partial^2 R_{0s}}{\partial \varphi'^2} D_3 + 2\frac{\partial R_{0s}}{\partial \varphi'}\frac{\partial D_3}{\partial \varphi'} + R_{ns}\frac{\partial^2 D_4}{\partial \varphi'^2}\end{array}\right] \quad \text{(C.1)}$$

$$\frac{\partial ds_h}{\partial n} = \frac{1}{s}\left[\begin{array}{c}\frac{\partial^2 R_{0h}}{\partial \varphi'^2} R_{nh} D_1 + 2\frac{\partial R_{0h}}{\partial \varphi'} R_{nh}\frac{\partial D_1}{\partial \varphi'} + R_{0s} R_{nh}\frac{\partial^2 D_1}{\partial \varphi'^2} + \frac{\partial^2 D_2}{\partial \varphi'^2} \\ + \frac{\partial^2 R_{0h}}{\partial \varphi'^2} D_3 + 2\frac{\partial R_{0h}}{\partial \varphi'}\frac{\partial D_3}{\partial \varphi'} + R_{nh}\frac{\partial^2 D_4}{\partial \varphi'^2}\end{array}\right] \quad \text{(C.2)}$$

Second derivative of the reflection coefficient with respect to φ' for soft and hard polarization are given by,

$$\frac{\partial^2 R_{0s}}{\partial \varphi'^2} = -2(\varepsilon_r - 1)\left(\frac{\sin\varphi' A(\sin\varphi' + A)^2 - \cos\varphi'\left(B(\sin\varphi' + A)^2 + 2A(\sin\varphi' + A)(\cos\varphi' + B)\right)}{(A^2)(\sin\varphi' + A)^4}\right) \quad \text{(C.3)}$$

$$\frac{\partial^2 R_{0h}}{\partial \varphi'^2} = -2\varepsilon_r(\varepsilon_r - 1)\left(\frac{\sin\varphi' A(\varepsilon_r \sin\varphi' + A)^2 - \cos\varphi'\left(B(\varepsilon_r \sin\varphi' + A)^2 + 2A(\varepsilon_r \sin\varphi' + A)(\cos\varphi' + B)\right)}{(A^2)(\varepsilon_r \sin\varphi' + A)^4}\right) \quad \text{(C.4)}$$

$$A = \sqrt{\varepsilon_r - cos^2(\varphi')} \quad , \quad B = \frac{\cos\varphi' \sin\varphi'}{\sqrt{\varepsilon_r - cos^2(\varphi')}}$$

Second derivative of the diffraction coefficient with respect to φ' is given by,

$$\frac{\partial^2 D_i}{\partial \varphi'^2} = \frac{-e^{-j\pi/4}}{2n\sqrt{2\pi k}} \left(\frac{\partial^2 \cot(\psi_i)}{\partial \varphi'^2} F(x_i) + 2 \frac{\partial \cot(\psi_i)}{\partial \varphi'} \frac{\partial F_{x_i}}{\partial \varphi'} + cot(\psi_i) \frac{\partial^2 F(x_i)}{\partial \varphi'^2} \right) \quad \text{(C.5)}$$

$$\frac{\partial^2 \cot(\psi_i)}{\partial \varphi'^2} = \frac{cos(\psi_i)}{2n^2 sin^3(\psi_i)}$$

Second derivative of the transition function with respect to φ' is given by,

$$\frac{\partial^2 F(x_i)}{\partial \varphi'^2} = \frac{\partial^2 x_i}{\partial \varphi'^2} \left(\frac{F(x_i)}{2x_i} + j(F(x_i) - 1) \right) + \frac{\partial x_i}{\partial \varphi'} \left[\left(\frac{x_i \frac{\partial F_{x_i}}{\partial \varphi'} - \frac{\partial x_i}{\partial \varphi} F(x_i)}{2{x_i}^2} \right) + j \frac{\partial F_{x_i}}{\partial \varphi'} \right] \quad \text{(C.6)}$$

$$\frac{\partial^2 x_i}{\partial \varphi'^2} = kLcos(2\psi_i)$$